Title: Integrating genetic regulation and single-cell expression with GWAS prioritizes causal genes and cell types for glaucoma

Authors:

Andrew R. Hamel[1,2,3], Wenjun Yan[4,*], John M. Rouhana[1,2,3,*], Aboozar Monovarfeshani[4,*], Xinyi Jiang[5,6], Puja A. Mehta[1,2,3], Jayshree Advani[7], Yuyang Luo[1,2,3], Qingnan Liang[8], Skanda Rajasundaram[2,9,10], Arushi Shrivastava[1,2,3], Katherine Duchinski[1,2,3], Sreekar Mantena[1,11], Jiali Wang[1,2,3], Tavé van Zyl[4,12], Louis R. Pasquale[13], Anand Swaroop[7], Puya Gharahkhani[14], Anthony P. Khawaja[15], Stuart MacGregor[14], International Glaucoma Genetics Consortium (IGGC), Rui Chen[8], Veronique Vitart[5], Joshua R. Sanes[4], Janey L. Wiggs[1,2,3], Ayellet V. Segrè[1,2,3,#]

Affiliations:

[1]Ocular Genomics Institute, Department of Ophthalmology, Massachusetts Eye and Ear, Boston, MA

[2]Department of Ophthalmology, Harvard Medical School, Boston, MA

[3]Broad Institute of Harvard and MIT, Cambridge, MA.

[4]Department of Molecular and Cellular Biology and Center for Brain Science, Harvard University, Cambridge, MA, USA

[5]MRC Human Genetics Unit, Institute of Genetics and Cancer, The University of Edinburgh, Edinburgh, UK

[6]Centre for Genomic and Experimental Medicine, Institute of Genetics and Molecular Medicine, The University of Edinburgh, Edinburgh, UK

[7]Neurobiology, Neurodegeneration and Repair Laboratory, National Eye Institute, National Institutes of Health, Bethesda, Maryland, USA

[8]Department of Molecular and Human Genetics, Baylor College of Medicine, TX

[9]Centre for Evidence-Based Medicine, University of Oxford, Oxford, UK

[10]Faculty of Medicine, Imperial College London, London, UK

[11]Harvard/MIT MD-PhD Program, Harvard Medical School, Boston, MA

[12]Department of Ophthalmology and Visual Sciences, Yale School of Medicine, New Haven, CT

[13]Department of Ophthalmology, Icahn School of Medicine at Mount Sinai, New York, NY, USA

[14]QIMR Berghofer Medical Research Institute, Brisbane, Queensland, 4029, Australia

[15]NIHR Biomedical Research Centre, Moorfields Eye Hospital NHS Foundation Trust and UCL Institute of Ophthalmology, London, UK

* Co-second authors, these authors contributed equally

[#] Correspondence to be addressed to Ayellet V. Segrè: ayellet_segre@meei.harvard.edu

Abstract

Primary open-angle glaucoma (POAG), characterized by retinal ganglion cell death, is a leading cause of irreversible blindness worldwide; however, the molecular and cellular causes are not well understood. Elevated intraocular pressure (IOP) is a major risk factor, but many patients have normal IOP. Colocalization and Mendelian randomization analysis of >240 POAG and IOP GWAS loci and of overlapping eQTLs and sQTLs in 49 GTEx tissues and retina prioritized causal genes for 60% of loci. These genes were enriched in pathways implicated in extracellular matrix organization, cell adhesion, and vascular development. Analysis of single-nucleus RNA-seq of glaucoma-relevant eye tissues revealed that the colocalizing genes and genome-wide POAG and IOP associations were enriched in specific cell types in the aqueous outflow pathways, retina, optic nerve head, peripapillary sclera, and choroid. This study nominated IOP-dependent and independent regulatory mechanisms, genes, and cell types that may contribute to POAG pathogenesis.

Introduction

Primary open-angle glaucoma (POAG) is the leading cause of irreversible blindness worldwide among people over the age of 55[1]. It is characterized by progressive optic neuropathy, caused by the gradual death of retinal ganglion cells (RGCs) that transmit visual information from the outer retina to the brain via the optic nerve (myelinated RGC axons)[2]. Elevated intraocular pressure (IOP) is a major risk factor for POAG[3] and is primarily caused by decreased outflow of the aqueous humor from the ocular anterior segment. Decreased outflow may be due to abnormal function of structures in the anterior segment of the eye, consisting of the trabecular meshwork (TM)[4] and Schlemm's canal (SC)[5] in the conventional outflow pathway, and the ciliary muscle and iris in the uveoscleral (unconventional) pathway[6]. However, about one third of patients with POAG display optic nerve degeneration in the absence of abnormally high IOP measurements (normal tension glaucoma (NTG))[7]. Conversely, many people with elevated IOP do not develop glaucoma, suggesting that other processes, including increased RGC susceptibility to normal IOP, might also lead to optic nerve damage. Currently, neuroprotective therapies are lacking, and medications that reduce IOP have limited effectiveness[2]. Gaining a better understanding of the molecular and cellular causes of POAG in the anterior and posterior segments of the eye could suggest novel therapeutic targets.

A recent multi-ethnic genome-wide association study (GWAS) meta-analysis of 34,179 POAG cases and 349,321 controls of European, Asian, and African ancestries identified 127 risk loci associated with POAG[8], explaining ~9% of POAG heritability, and a meta-analysis of the European subset identified 68 POAG loci[8], some of which were not uncovered in the cross-ancestry meta-analysis. Furthermore, a GWAS meta-analysis of IOP performed on 139,555 individuals, primarily of European descendant[9], has identified 133 independent associations in 112 loci, largely overlapping with two other studies[10,11]. The IOP variants' effect sizes and direction of effect are highly correlated with their effect on POAG risk[8,9], and together they explain 9-17% of IOP heritability. Vertical-cup-to-disc ratio (VCDR), central corneal thickness, and corneal hysteresis, a measure of the viscoelastic damping of the cornea, have also been associated with POAG risk, and large GWAS meta-analyses have uncovered 70-200 genetic associations for these traits[12–23].

Identifying putative causal genes and cell types underlying the genetic associations with POAG and its related traits is challenging. As with other complex traits, a majority of associated variants lie in noncoding regions and are enriched for regulatory effects[24–26]. Due to linkage disequilibrium (LD), the discovered associations typically tag multiple variants and genes, making it hard to pinpoint the implicated causal gene(s) from sequence alone. Furthermore, genetic regulatory effects in relevant ocular tissues are limited, reported to date only in retinal tissues[27–30], and have not yet been detected at cellular resolution in other parts of the eye. Nevertheless, through single-cell or single-nucleus RNA-sequencing (sc/snRNA-seq), human cell atlases and cellular level transcriptomes have been generated for various non-diseased eye tissues relevant to POAG pathogenesis, including retina[31–33], the aqueous humor outflow pathways[34,35], six tissues in the anterior chamber[36], and the optic nerve head (ONH), where RGCs pass to exit the eye, the optic nerve, and surrounding posterior tissues[37]. Using a method we recently developed, ECLIPSER[38,39], we show that cell type-specific enrichment of genes mapped to GWAS loci of complex diseases and traits can help identify cell types of action for diseases in relevant tissues[38,39].

In this study, we have combined expression quantitative trait loci (eQTLs) and splicing QTLs (sQTLs) in 49 (non-ocular) tissues from the Genotype-Tissue Expression (GTEx) Project[26], retinal eQTLs[31,32], retinal Hi-C data[40], and single-cell expression from glaucoma-relevant eye tissues[33,36,37] with POAG and IOP genetic associations to identify regulatory mechanisms, genes, pathways, and cell types that may play an important role in POAG etiology.

Results

An overview of the analytical steps and approaches taken are described in Fig. 1 and Supplementary Note.

103 **POAG and IOP associations enriched among eQTLs and sQTLs.** To assess the relevance of
104 eQTLs and sQTLs to POAG risk and IOP variation, we tested whether *cis*-eQTLs and *cis*-sQTLs
105 (e/sQTLs) from 49 GTEx (v8) tissues[26] and peripheral retina *cis*-eQTLs[27,28] were enriched for POAG
106 or IOP associations (GWAS P<0.05) using *QTLEnrich*[24,26] that adjusts for confounding factors and
107 tissue sample size (Methods and Fig. 1a). We found significant enrichment of multiple POAG and
108 IOP associations (both genome-wide significant and subthreshold) among eQTLs and sQTLs in
109 most of the 49 GTEx tissues and in retina (Bonferroni-corrected $P<5x10^{-4}$) (Fig. 2a, b and
110 Supplementary Tables 1-3). Many of the top enriched GTEx tissues contain cell types that may be
111 pathogenic to glaucoma (Supplementary Note). The relative contribution of sQTLs to POAG and
112 IOP, as measured by adjusted fold-enrichment and estimated true positive rate, was larger than
113 the relative contribution of eQTLs to these traits (One-sided Wilcoxon rank sum test $P<1.5x10^{-11}$
114 and P<0.03, respectively; Supplementary Fig. 1a-c, and Supplementary Tables 1-3), as observed
115 with other complex traits[26]. The absolute number of eQTLs proposed to contribute to POAG and
116 IOP (average 258 to 606 per tissue) was 2-fold larger than that of sQTLs (average 124 to 320 per
117 tissue), likely due to the larger discovery rate of eQTLs compared to sQTLs[26] (Supplementary Fig.
118 1a-c and Supplementary Table 1). The target genes of eQTLs or sQTLs with top-ranked POAG or
119 IOP GWAS p-values (P<0.05) were enriched in metabolic and cellular processes (Methods;
120 Supplementary Tables 4-5; Supplementary Note).
121
122 **Colocalization analysis of POAG and IOP GWAS loci with *cis*-e/sQTLs.** Given the widespread
123 e/sQTL enrichment of POAG and IOP associations, we used the e/sQTLs in all 49 GTEx tissues
124 and retina eQTLs to propose putative causal genes that may underlie genome-wide significant loci
125 for these traits. We applied two colocalization methods, eCAVIAR[41] and *enloc*[42], to 127 POAG loci
126 from a large cross-ancestry GWAS meta-analysis[8], 68 POAG loci from a European (EUR) subset
127 meta-analysis[8] (POAG EUR), and 133 IOP loci from a primarily European GWAS meta-analysis[9]
128 (IOP) (variant list in Supplementary Table 6; Methods and Fig. 1a), and any e/sQTLs that
129 overlapped each GWAS locus LD interval (Methods). The results are presented per trait and
130 colocalization method in Supplementary Tables 7-12 and summarized in Supplementary Table 13.
131 We defined a "comprehensive set" of putative causal genes and regulatory mechanisms for POAG
132 and IOP as those e/sGenes that were significant with at least one of the colocalization methods
133 (Colocalization posterior probability (CLPP) > 0.01 for eCAVIAR, and regional colocalization
134 probability (RCP) > 0.1 for *enloc* (see Methods); Supplementary Table 13), filtering out potential
135 false positives (See Methods and examples in Supplementary Fig. 3). The largest number of
136 colocalizing e/sGenes was found in tibial nerve, adipose, skin, artery, and fibroblasts, among other

137 tissues, many of which contain cell types relevant to the pathogenicity of glaucoma (Supplementary
138 Fig. 4). Eighteen retina eQTLs colocalized with 13 POAG and/or IOP loci (Column AH in
139 Supplementary Table 13). The number of significantly colocalizing e/sGenes per tissue significantly
140 correlated with tissue sample size (Pearson's R^2=0.72, P=1x10^{-14}, Supplementary Fig. 4) that is
141 also associated with the number of detected e/sQTLs per tissue[26]. This suggests that e/sQTL
142 discovery power is a driving factor in tissue identity of the colocalizing e/sQTLs. We therefore
143 primarily considered the causal genes proposed by the colocalization analysis and not the
144 associated tissues, in downstream analyses.
145 We found that 58% of all GWAS loci tested significantly colocalized with at least one eQTL
146 and/or sQTL based on eCAVIAR and/or *enloc*: 60% (76) of 127 cross-ancestry POAG GWAS loci,
147 53% (36) of 68 European POAG loci and 59% (79) of 133 IOP loci (Fig. 2c and Supplementary
148 Table 14). About 55% and 29% of GWAS loci colocalized with ≥1 eQTL and ≥1 sQTL, respectively.
149 For 21% of the POAG and IOP GWAS loci (69 loci total), significant colocalization was found for
150 the same e/sGene with eCAVIAR and *enloc* ('high confidence set' listed in Table 1 and
151 Supplementary Table 15). The GWAS-e/sQTL colocalization analysis significantly reduced the
152 number of putative causal genes per GWAS locus for POAG and IOP from an average of 22.8 ±
153 1.8 genes tested per LD interval (range: 3-166, median=15) to an average of 3.5 ± 0.4 genes per
154 locus (range: 1-36, median of 1 or 2 genes per locus per trait; Fig. 2d,e and Supplementary Table
155 16). eQTLs and sQTLs nominated an average of 3 and 2 causal genes per locus, respectively, with
156 partial overlap of target genes between the colocalizing eQTLs and sQTLs (Fig. 2e and
157 Supplementary Table 16). 60-72% of the colocalizing e/sGenes per trait were protein-coding and
158 18-20% were noncoding RNA genes, half of which were lincRNAs and half antisense genes (Fig.
159 2f, Supplementary Tables 17-18, and Supplementary Note). A single causal gene was proposed
160 for 80 (42%) of the POAG and IOP loci with significantly colocalizing e/sQTLs (Supplementary
161 Tables 19-20), 49 (61%) of which are the nearest gene to the lead GWAS variant. In 30.3% (23/76),
162 16.7% (6/36) and 31.7% (25/79) of the POAG cross-ancestry, POAG EUR and IOP GWAS loci,
163 respectively, with significant colocalization results, the colocalizing e/sGenes were not the nearest
164 gene to the lead GWAS variant. In total, 228, 118, and 279 genes, including previously suggested
165 and novel ones, are candidate causal genes for POAG cross-ancestry risk, POAG EUR risk, and
166 IOP variation, respectively (Supplementary Table 21), with a total of 459 genes proposed from the
167 combined datasets.
168
169 **Colocalizing e/sGenes of top POAG and IOP GWAS loci and direction of regulatory effect**
170 **on disease risk.** In addition to prioritizing causal genes and regulatory mechanisms that may

171 contribute to POAG and IOP, colocalizing e/sQTLs propose the direction of effect of altered gene
172 expression or splicing on disease risk or trait variation (examples for top POAG and IOP GWAS
173 signals in Fig. 3 and Supplementary Fig. 5). For example, an eQTL and sQTL acting on *TMCO1*
174 and an eQTL acting on *TMCO1*'s antisense, *RP11-466F5.8*, in the opposite direction, colocalized
175 with the second strongest association with POAG (rs2790053, odds ratio (OR)=1.35; CLPP=0.92-
176 1) and the top IOP association (rs116089225, beta = -0.744; CLPP=0.87-1) (Fig. 4a-e and
177 Supplementary Fig. 6). Decreased expression of *TMCO1* and increased expression of *RP11-*
178 *466F5.8* are proposed to lead to increased IOP levels and increased POAG risk (Fig. 4,
179 Supplementary Fig. 6, and Supplementary Table 13). Furthermore, an alternative splice donor site
180 in exon 4, the first exon in the *TMCO1* mRNA in GTEx Cells Cultured fibroblasts, leads to a longer
181 exon 4 (Fig. 4f,g) that is associated with decreased POAG risk (Supplementary Tables 7 and 13).
182 *TMCO1* is expressed in different cell types in the anterior and posterior parts of the eye, including
183 lymphatic and fibroblast cells in the conventional and unconventional outflow pathways, vascular
184 and immune cells in the anterior and posterior segments, and macroglial cells in the retina
185 (Supplementary Figure 7). Other examples include *ANGPT1* and *ANGPT2*, involved in vascular
186 biology, whose increased expression is proposed to reduce IOP levels (Supplementary Fig. 8 and
187 Supplementary Table 13) that is consistent with the effect observed on IOP in *Angpt1*-knockout
188 mice[43].
189
190 **Colocalizing genes for shared and distinct POAG and IOP loci.** Of 50 overlapping POAG and
191 IOP GWAS loci, 39 (78%) of the loci had at least one significant colocalization result for both traits,
192 and in all cases at least one common gene was implicated (Supplementary Table 13 and Table 1).
193 In most of the cases (95%), the relative direction of effect of the colocalizing e/sQTLs on IOP was
194 consistent with IOP's effect on POAG risk, proposing IOP-dependent mechanisms for POAG risk.
195 For example, decreased *GAS7* expression or increased *ABO* expression were associated with both
196 increased IOP levels and increased POAG risk (Supplementary Tables 7-13 and Supplementary
197 Figs. 9-10). e/sGenes that colocalize with POAG loci not associated with IOP (48 loci; Column N
198 in Supplementary Table 13) may suggest IOP-independent mechanisms.
199 To prioritize regulatory variants and genes that may affect POAG independent of IOP, we
200 integrated retina Hi-C loops and/or epigenetically derived *cis*-regulatory elements (CREs) and
201 super-enhancers (SEs) (Supplemental Data 4 in Marchal *et al*.[40]) with the POAG-only loci
202 (Methods). In 17 of the loci, ≥1 colocalizing e/sQTLs was supported as a potential causal
203 mechanism by retina Hi-C loops (6 loci), CREs (16 loci) and/or SEs (5 loci) (Supplementary Table
204 22). This includes the strongest normal tension glaucoma (NTG) association (9p21)[8,44] in the POAG

205 cross-ancestry (rs944801 OR=1.26) and POAG EUR (rs6475604 OR=1.3) GWAS meta-analyses
206 that colocalized with a *CDKN2A* eQTL in brain cortex, *CDKN2B-AS1 and RP11-149I2.4* sQTLs in
207 pituitary, and *CDKN2B* eQTL in skeletal muscle (Supplementary Table 13). The POAG risk variants
208 and colocalizing e/sQTLs in this locus overlapped retinal CREs (Fig. 5a). These results imply that
209 increased expression of *CDKN2A,* decreased expression of *CDKN2B*, and exon skipping in
210 *CDKN2B-AS1* may increase POAG risk (Fig. 3, Supplementary Figs. 5a and 11). Other examples,
211 involving a retina *SLC2A12* eQTL overlapping a retinal CRE, and e/sQTLs acting on *RERE* and its
212 antisense, *RERE-AS1*, that are physically linked via retina chromatin loops to the *RERE*
213 transcription start site (TSS), are shown in Fig. 5b and c (see also Supplementary Table 22).
214 Notably, *RERE* expression is enriched in oligodendrocytes in the optic nerve head and optic nerve
215 (False discovery rate (FDR)=0.07) and in retinal pigment epithelium (RPE) and S-cones in the
216 macula (FDR=0.06), as shown below (Supplementary Table 38; Supplementary Fig. 18f, g).
217
218 **Colocalizing genes in population-specific and cross-ancestry POAG loci.** For all 59 POAG
219 EUR loci also found in the POAG cross-ancestry meta-analysis, at least one common colocalizing
220 e/sGene was found for both the EUR and cross-ancestry GWAS (Supplementary Table 13). One
221 such example is *EFEMP1*, in which rare mutations have been associated with a Mendelian form of
222 glaucoma[45]. Colocalization analysis suggests that skipping of exons 6 and 7 in *EFEMP1* may be
223 protective for POAG (Supplementary Fig. 12). Of the 9 loci found only in the POAG EUR GWAS,
224 two loci colocalized with eQTLs acting on several genes each, including genes involved in the
225 extracellular matrix (*EMID1*) and vascular endothelial growth (*ANGPTL2*), respectively, both of
226 which also colocalized with IOP (Supplementary Table 23). In addition, three associations in the
227 POAG cross-ancestry meta-analysis demonstrated significant allelic heterogeneity among the
228 three populations (European, East Asian, and African American)[8]. e/sQTL colocalized with two of
229 these loci. One is the 9p21 locus rs944801 with *CDKN2A/B* described above, which was significant
230 in the European and Asian populations, but not the African population (P_heterogeneity=1.5 x 10^{-}
231 ^{8}) in which it is in lower frequency (AFR MAF=0.073, EUR MAF=0.42, EAS MAF=0.11 in gnomAD
232 (URLs)). The other is a European-specific locus with the largest POAG odds ratio (rs74315329,
233 OR=5.47). This variant is a nonsense mutation (p.Gln368Ter) in *MYOC*, known to cause juvenile-
234 onset and adult-onset open-angle glaucoma with dominant inheritance[46]. This variant is 10-fold
235 more common in the European population compared to the African population and is not found in
236 the East Asian population (gnomAD; URLs). Of all the e/sQTL gene-tissue pairs that overlapped
237 this locus targeting 24 genes, we identified an sQTL acting on *PIGC,* phosphatidylinositol glycan
238 anchor biosynthesis class C, that significantly colocalized with the POAG cross-ancestry locus

239 (spleen CLPP=0.12, and arterial tissues RCP=0.26-0.34; Supplementary Table 13 and
240 Supplementary Fig. 13). Conditioning on the nonsense variant in *MYOC* that is likely the primary
241 causal variant in the locus, we found that a secondary haplotype colocalized with the *PIGC* sQTL
242 (Supplementary Tables 24-28; more details in Supplementary Note). These results suggest that
243 decreased exon 2 skipping in *PIGC* or increased *PIGC* expression may lead to increased POAG
244 risk (Supplementary Fig. 13). *PIGC* is among 10 colocalizing POAG genes enriched in
245 oligodendrocytes in the optic nerve head and optic nerve (See below; FDR=0.07, Supplementary
246 Table 38; Supplementary Fig. 18f, g).
247
248 **Mendelian randomization (MR) of colocalizing e/sQTLs**. To provide additional support for a
249 causal relationship between e/sQTLs and POAG and/or IOP, we applied two-sample MR to all the
250 significantly colocalizing e/sQTL and GWAS locus pairs based on eCAVIAR and/or *enloc*
251 (Methods). We found evidence for a causal relationship (FDR < 0.05) for 348 (75%) genes that
252 were robust to the influence of horizontal pleiotropy, where pleiotropy-robust sensitivity could be
253 performed (Supplementary Table 29). A high-confidence list of putative POAG and/or IOP causal
254 genes based on colocalization analysis and MR is provided in Table 1. We found 239 e/sGenes to
255 have significant MR associations with both POAG and IOP, including *TMCO1, GAS7,* and *LMX1B,*
256 which colocalized with the largest association signals for both POAG and IOP GWAS loci
257 (Supplementary Figs. 5, 6, 9), and *DGKG* and *NPC2*, whose retina eQTLs colocalized with POAG
258 and IOP. Sixty-eight genes had significant MR associations with IOP but not POAG, such as *HLA-*
259 *B* and *SLC7A6*, and 41 genes had significant MR associations with POAG but not IOP, such as
260 *CDKN2B-AS1, RERE, and YAP1*, proposing high-confidence IOP-independent mechanisms
261 (Supplementary Table 29 and Fig. 5). Since the MR analysis could not be applied to the larger,
262 better-powered POAG cross-ancestry GWAS, as it requires a similar population background
263 between the e/sQTL and GWAS studies (European in our case), our downstream analyses were
264 applied to the more inclusive list of proposed causal genes based on the colocalization analysis
265 (Supplementary Table 13).
266
267 **Enrichment of POAG and IOP colocalizing e/sGenes in biological processes.** To gain
268 biological insight into ways the implicated genes might contribute to glaucoma pathogenesis, we
269 next tested whether the target genes of all the colocalizing e/sQTLs with POAG cross-ancestry,
270 POAG EUR, or IOP GWAS loci were enriched in specific biological pathways, gene ontologies, or
271 mouse phenotype ontologies, using *GeneEnrich* (Methods and Fig. 1c). Genes that colocalized
272 with POAG cross-ancestry loci were significantly enriched in elastic fiber formation (Empirical P-

273 value (P)<$1x10^{-5}$, FDR<0.001) and extracellular matrix organization (P=$3x10^{-5}$, FDR=0.012), and
274 nominally enriched (P<0.05) in the transforming growth factor beta (TGF) receptor signaling
275 pathway (P=$3x10^{-4}$) and abnormal eye morphology (P=$2.6x10^{-3}$), amongst others (Supplementary
276 Table 30 and Supplementary Fig. 14a,b). Genes that colocalized with POAG EUR loci were
277 nominally enriched (P < $4x10^{-3}$) in cellular senescence and cell cycle processes (e.g., Cyclin D-
278 associated events in G1), lipid-related processes, such as apolipoprotein binding and decreased
279 circulating high-density lipoprotein cholesterol level, and retina or neuronal related processes,
280 including abnormal retina morphology, abnormal sensory neuron innervation pattern, and negative
281 regulation of axon extension involved in axon guidance (Supplementary Table 31 and
282 Supplementary Fig. 14c,d).
283 For the IOP genes, significant enrichment (P=$2x10^{-5}$, FDR=0.025) was found in
284 transcriptional regulation by *VENTX*, a gene that encodes a homeodomain-containing transcription
285 factor (Supplementary Table 32 and Supplementary fig. 14e). *VENTX* and its IOP-colocalizing
286 target genes driving the gene set enrichment signal (*ANAPC1*, *ANAPC7*, *AGO4*, *MOV10*, *TCF7L2*)
287 were most highly expressed in immune cell types, lymphocytes and macrophages, in the single cell
288 anterior segment and optic nerve head described below (Supplementary Fig. 14f). The IOP genes
289 were also significantly enriched (FDR<0.15) in blood vessel morphogenesis and vasculature
290 development, regulation of cytoskeletal organization, negative regulation of cellular component
291 organization, and adherens junction (Supplementary Table 32 and Supplementary Fig. 14e). Since
292 colocalization with multiple e/sQTLs was found for two GWAS loci in the HLA region on
293 chromosome 6 associated with POAG and IOP (29 and 35 e/sGenes, respectively), likely due to
294 high LD in the HLA region, we removed this region from the gene set enrichment analysis above
295 to avoid inflating the results due to a single locus. When kept in, the endosomal vacuolar pathway,
296 interferon gamma signaling, antigen presentation folding assembly and peptide loading of class I
297 MHC, negative regulation of natural killer cell-mediated immunity, and cell aging were significantly
298 enriched (FDR<0.1) for POAG genes (Supplementary Table 33), in addition to the gene sets above.
299 The colocalizing POAG and IOP genes driving the gene set enrichment signals are listed in
300 Supplementary Tables 30-33.
301
302 **Identifying pathogenic cell types for POAG and related ocular traits.** To further relate the
303 implicated genes to pathogenic mechanisms and cell types, we next tested whether the expression
304 of POAG or IOP colocalizing e/sGenes was enriched in specific cell types in key eye tissues
305 implicated in the pathophysiology of POAG. We first applied ECLIPSER[38,39] (Methods and Fig. 1d)
306 to 228, 118, and 279 e/sGenes that colocalized with POAG cross-ancestry, POAG EUR and IOP

307 GWAS loci, respectively (Supplementary Tables 13 and 34), and to cell type-specific expression
308 from single nucleus (sn) RNA-seq of 13 tissues dissected from non-diseased human eyes: central
309 cornea, corneoscleral wedge (CSW), trabecular meshwork (TM) including Schlemm's canal, iris,
310 ciliary body (CB), lens[36] (all from anterior segment), peripheral and macular retina[33,36], the optic
311 nerve head (ONH), optic nerve (ON), peripapillary sclera (PPS), peripheral sclera, and choroid[37]
312 (all from posterior segment) (Methods and Supplementary Tables 35-37). The cell type enrichment
313 results are summarized in Supplementary Table 38.

314 In the anterior segment, we found significant enrichment (tissue-wide FDR<0.1) for POAG
315 EUR loci in fibroblasts derived from the ciliary muscle (present in CB, CSW and TM[36]), annotated
316 as ciliary fibroblasts in van Zyl *et al.*[36], followed by fibroblasts derived from the iris root (present
317 within the iris[36]), annotated as iris fibroblasts (Supplementary Table 38 and Fig. 6a,b). The ciliary
318 muscle and iris are key tissues involved in the unconventional outflow pathway. These fibroblasts
319 were also detected histologically within the TM where all three tissues meet and interweave at the
320 iridocorneal angle[36], implicating the conventional aqueous outflow pathway as well. Fig. 6c shows
321 the e/sGenes driving the POAG EUR enrichment signal in ciliary fibroblasts. The POAG EUR genes
322 were also modestly enriched in fibroblasts derived predominantly from the TM tissue (annotated as
323 TM fibroblasts[36]) (P=0.014, FDR=0.18). For POAG cross-ancestry and IOP loci, we found
324 supportive enrichment (P<0.05, FDR<0.23) in outflow pathway and cornea fibroblasts, vascular
325 endothelium cells (cluster 2 derived from TM, CSW and CB tissues[36]), and lens epithelium, as
326 detailed in Fig. 6a,d,e and Supplementary Table 38. Genes that colocalized with IOP loci were also
327 significantly enriched (FDR<0.1) in pericytes (cluster 2 that localizes to the CSW[36]), and nominally
328 enriched in lymphatic endothelium and Schlemm's canal, whose dysfunction can lead to elevated
329 IOP[47] (Fig. 6e and Supplementary Table 38).

330 Clustering of the top-ranked anterior segment cell types (P<0.05) for POAG and IOP,
331 separately, based on the overlap of genes driving the cell type enrichment, suggests three cell
332 classes affecting POAG - fibroblasts, vascular endothelium, and lens epithelium; and three cell
333 classes for IOP - fibroblasts, pericytes, and lymphatic endothelial cells (Fig. 6f, g). Between 45-
334 78% of the genes driving the POAG enrichment signals in the outflow fibroblast cell types are
335 common between the different fibroblasts (Fig. 6f), suggesting both shared and distinct genes
336 acting in the conventional and unconventional outflow pathways. The IOP genes driving the
337 enrichment signal in pericytes (Fig. 6h,i) were largely distinct from those enriched in vascular and
338 fibroblast cell types (overlap 7-33%; Fig. 6g), and were enriched in vasculature development
339 ($P=3x10^{-5}$, FDR=0.075; Supplementary Table 40). On the other hand, the IOP genes driving the
340 enrichment in TM fibroblasts (Supplementary Fig. 15c,d) were highly shared with the IOP genes

341 enriched in ciliary and iris fibroblasts (overlap 64-88%; Fig. 6g). Notably, the enrichment of IOP
342 genes in pericytes was specific to IOP (asterisks in Fig. 6h). When ECLIPSER was applied to genes
343 that colocalized with IOP loci not associated with POAG, only the enrichment in pericytes remained
344 (P=0.007) (Supplementary Table 41 and Supplementary Fig. 15e). Genes mapped to shared IOP
345 and POAG loci were significantly enriched in ciliary and TM fibroblasts (FDR<0.01) and lymphatic
346 or vascular endothelial cells (FDR=0.026). No enrichment was found for POAG-only loci in the
347 anterior segment cell types, supporting IOP-dependent mechanisms in the anterior segment for
348 POAG risk, as expected (Supplementary Table 41).

349 We next tested for enrichment of POAG and IOP colocalizing e/sGenes in retina snRNA-
350 seq data (Methods). We found significant enrichment of POAG cross-ancestry genes in astrocytes
351 and Müller glia cells (FDR<0.04; Supplementary Table 38, Fig. 7a and Supplementary Fig. 16a),
352 which replicated (FDR<0.06) in a separate snRNA-seq study of the macula (Methods;
353 Supplementary Table 38 and Supplementary Fig. 16g). Consistent results were found for POAG
354 EUR genes (Supplementary Fig. 16b). A quarter (*YAP1, LPP, TRIB2)* of the 12 POAG cross-
355 ancestry genes driving the astrocyte enrichment were common with Müller glia cells
356 (Supplementary Fig. 16d, e), suggesting both shared and distinct processes between the two cell
357 types. IOP genes were only nominally enriched in astrocytes (P=0.032; Supplementary Fig. 16c).
358 By testing POAG- or IOP-only loci and shared loci, the POAG enrichment in retinal astrocytes and
359 Müller glia cells appears to be independent of IOP (Supplementary Table 41 and Supplementary
360 Fig. 17; more details in Supplementary Note). The POAG cross-ancestry genes were also enriched
361 in RPE cells and S-cones in the macula (FDR=0.06). Of note, no significant enrichment was
362 observed in RGCs (Fig. 7a), though some POAG colocalizing e/sGenes are expressed in RGCs
363 (Supplementary Fig. 20).

364 Finally, we tested for cell type-specific enrichment in the optic nerve head (ONH), optic
365 nerve (ON) and adjacent posterior tissues (Methods; Supplementary Table 37). The strongest
366 enrichment (FDR<0.01) of POAG cross-ancestry genes was found in fibroblasts primarily in the
367 peripapillary sclera (PPS) that encompasses the ONH, followed by fibroblasts most abundant in
368 the choroid, astrocytes that reside in the ONH and ON, Schwann cells in the choroid and PPS,
369 oligodendrocyte precursor cells (OPCs) and oligodendrocytes in the ON and ONH (Supplementary
370 Fig. 18f,g), and vascular endothelium cells primarily in the choroid (FDR<0.09; Fig 7b,c,
371 Supplementary Table 38 and Supplementary Fig. 18a,d). POAG EUR genes showed similar
372 enrichment patterns (Fig. 7b, Supplementary Fig. 18b and Supplementary Table 38). About half
373 the genes driving the enrichment in astrocytes in ONH (Fig. 7d, e) and retina samples from separate
374 donors were common (e.g., *DGKG, PLCE1, LPP*, *GAS7*, *YAP1*, and *COL11A1*; Supplementary

375 Table 38). *DGKG*, diacylglycerol kinase gamma, whose retina-specific eQTL colocalized
376 (CLPP=0.96) with POAG cross-ancestry association (Fig. 7f) displayed the strongest cell type
377 specificity in ONH (Fig. 7d) and retinal astrocytes (Supplementary Fig. 16d).

378 IOP genes were most significantly enriched in vascular endothelial cells and fibroblasts
379 primarily residing in the choroid, but also in the ONH and PPS (FDR<0.014), followed by Schwann
380 cells in the choroid and PPS, vascular smooth muscle cells (19-ACTA2; Supplementary Fig. 18h,i)
381 in the PPS and sclera, pericytes (26-ACTA2) in the ONH, PPS and choroid, and OPCs in the ON
382 (FDR<0.06; Fig. 7b, Supplementary Table 38, and Supplementary Fig. 18a,c,e). The IOP genes
383 driving enrichment in vascular endothelial cells in the ONH, choroid and posterior tissues were
384 enriched in vasculature development and anchoring junction gene ontologies (FDR<0.06), and IOP
385 genes enriched in pericytes in the ONH, choroid and PPS were enriched in TIE2 signaling
386 (FDR=0.02), response to carbohydrate adhesion (FDR=0.13), and negative regulation of cell
387 adhesion (FDR=0.13) (Supplementary Table 40). Notably, the enrichment in oligodendrocytes and
388 OPCs was specific to POAG-only loci, and enrichment in vascular endothelium and mural cells was
389 specific to IOP-only loci (Supplementary Table 41 and Supplementary Fig. 19).

390 The cell type expression profiles of all POAG cross-ancestry, POAG EUR and IOP
391 colocalizing e/sGenes is shown in Supplementary Fig. 20, and a summary of the cell types and
392 pathways in which each of the POAG and IOP colocalizing e/sGenes are enriched is presented in
393 Supplementary Tables 42-44. Applying ECLIPSER to various negative control traits suggests that
394 the cell type enrichment results are specific to glaucoma and not due to unaccounted confounding
395 factors (Supplementary Tables 45-46, Fig. 6a, and Supplementary Fig. 21; Supplementary Note).
396 Furthermore, the ECLIPSER cell type enrichment significance did not correlate with cell count per
397 cell type in the single-nucleus datasets (Pearson's R^2<0.2, P>0.12; Supplementary Table 47).

398 To increase confidence in the POAG and IOP cell type enrichment results, we applied two
399 additional methods that identify cell types associated with complex traits, through regression
400 analysis of genome-wide associations beyond known GWAS loci: stratified LD score regression
401 (S-LDSC) and MAGMA (Fig. 1e; Methods). The primary enriched cell types for POAG and IOP
402 found with ECLIPSER, including ciliary and TM fibroblasts, ONH fibroblasts, and retinal macroglial
403 cells, were significant with S-LDSC (Supplementary Table 48; Supplementary Fig. 22) and more
404 restrictively with MAGMA (Supplementary Table 49; Supplementary Fig. 22); additional enrichment
405 was found in vascular types. Enrichment of POAG loci in ONH and ON oligodendrocytes was only
406 found with ECLIPSER suggesting that the enrichment is primarily driven by genes with strong
407 genetic effects. The cell type enrichment significance of ECLIPSER was reasonably correlated with
408 that of S-LDSC and MAGMA (Average Pearson's r=0.53, range: 0.18-0.86; Supplementary Table

409 50). We further used conditional analysis implemented in MAGMA to test whether the different cell
410 type enrichment signals for POAG or IOP were independent of each other in each tissue
411 (Supplementary Table 51). In the anterior segment, the enrichment of POAG associations in ciliary
412 fibroblasts was independent of TM fibroblasts, but not vice versa (Conditional P=0.04). In retina,
413 POAG associations were significantly enriched in astrocytes (P<6E-8) and Müller glia cells
414 (P<0.002), but only astrocytes remained significant after conditional analysis (Conditional P<4E-6),
415 suggesting that astrocytes may play a more important role in glaucoma pathogenicity than Müller
416 Glia cells. In the ONH, the POAG and IOP enrichment in fibroblasts, astrocytes, vascular
417 endothelium, and mural cells were all independent of each other (Supplementary Table 51).
418 Finally, to augment the POAG and IOP enrichment analysis, we tested for cell type
419 enrichment of genes mapped to GWAS loci of additional glaucoma associated traits (listed in
420 Supplementary Table 34), including vertical-cup-to-disc ratio (VCDR), cornea hysteresis, and
421 central cornea thickness (Methods) in all ocular tissue regions (Supplementary Table 38, Fig. 6a
422 and Fig. 7a, b). In the anterior segment, genes mapped to central corneal thickness and corneal
423 hysteresis were most significantly enriched in corneal fibroblasts (FDR<0.007; Fig. 6a and
424 Supplementary Fig. 23a, b), highlighting the specificity of the POAG and IOP gene enrichment in
425 the outflow pathway fibroblasts. The VCDR GWAS loci from a well-powered GWAS that used deep
426 learning (ML) to score the characteristics of fundus images from 65,680 European individuals[12]
427 showed significant enrichment in the TM fibroblasts from the conventional outflow pathway
428 (FDR=0.02; Fig. 6a and Supplementary Fig. 23c). TM fibroblasts were also the top nominally
429 enriched cell type for a smaller VCDR GWAS, where 23,899 fundus images were manually scored
430 by ophthalmologists[13] (P=0.0076, FDR=0.3; Fig. 6a and Supplementary Fig. 23d). In the retina, the
431 ML-based VCDR loci displayed significant enrichment in GABAergic amacrine cells, cone
432 photoreceptors and Müller glia cells (FDR<0.085; Fig. 7a and Supplementary Fig. 23e) and nominal
433 enrichment in astrocytes. In the ONH, the ML-based VCDR genes were nominally enriched in
434 fibroblasts in the PPS, vascular endothelium primarily in the choroid, and astrocytes in the ONH
435 and ON, similarly to POAG loci (Fig. 7b and Supplementary Fig. 23g, h; Supplementary Table 38).
436 In summary, our cell type enrichment analysis has revealed roles for both known and less
437 well-studied cell types in POAG pathogenicity, such as fibroblasts in the unconventional and
438 conventional outflow pathways, astrocytes in retina and ONH, OPCs in the ON and ONH, and
439 Schwann cells and fibroblasts in the PPS and choroid. It also suggests known and new causal
440 genes for POAG and related eye traits that may be affecting glaucoma susceptibility through
441 specific cell types in the anterior and posterior parts of the eye in IOP-dependent and independent
442 manners (Supplementary Tables 38 and 41).

443 **Discussion**

444

445 We report results of a systematic investigation of the underlying causal mechanisms, genes
446 and cell types of over 130 cross-ancestry or European loci associated with POAG[8,9] and over 110
447 loci associated with its major risk factor, elevated IOP[9]. Our analysis integrated a variety of
448 datasets, including expression and splicing QTLs from 49 GTEx tissues[26] and from retina[26,27],
449 genome topology data from retina[40], single-nucleus expression data from a whole-eye cell atlas
450 that includes key structures of both the anterior[36] and posterior segments[33,37], and the largest to
451 date GWAS meta-analyses for these traits[8,9]. Our finding that eQTLs and sQTLs in GTEx tissues
452 and retina are enriched for hundreds of known and more modest POAG and IOP associations,
453 suggests a primary role for transcriptional regulation in POAG susceptibility, as observed for other
454 diseases[24–27], and implies that GTEx tissues can be used to uncover causal mechanisms for
455 glaucoma. The GTEx e/sQTLs likely capture shared genetic regulation with the actual pathogenic
456 tissues for glaucoma, such as fibroblasts and vascular endothelial cells, as well as shared
457 regulation across cell types and tissues[26].

458 Using two QTL/GWAS colocalization methods[41,42], we prioritized putative causal genes for
459 ~60% of the POAG and IOP GWAS loci. A similar fraction of GWAS loci with significant
460 colocalization results has been found for other complex diseases and traits[26,48]. For a quarter (80)
461 of the POAG and IOP loci, a single gene was proposed, ten of which are noncoding genes (lincRNA
462 and antisense), suggesting that transcriptional and post-transcriptional gene regulation contribute
463 to glaucoma susceptibility. We provided additional support for three quarters of the colocalizing
464 e/sGenes using Mendelian randomization[49,50,51], which tests for horizontal pleiotropy, not accounted
465 for by Bayesian colocalization analysis[52,53]. For about one third of the GWAS loci, none of the
466 proposed causal gene/s were the nearest gene to the lead GWAS variant, similar to that observed
467 for other complex traits[24,48,54]. These results emphasize the value of using e/sQTLs or other
468 functional assays that link regulatory regions to distal target genes[24,55–57] to prioritize causal genes
469 underlying common variant associations.

470 Integrating e/sQTLs with POAG and IOP GWAS loci proposed both previously suggested[8]
471 and new biological processes for these traits. The POAG colocalizing genes, which included
472 several known mendelian, early-onset glaucoma genes (*EFEMP1*[45,58] and *LTBP2*[59]), were most
473 strongly enriched in extracellular matrix organization and elastic fiber formation, as previously
474 reported[8], followed by TGF receptor signaling pathway. Structural changes of the extracellular
475 matrix induced by TGF-beta2 in both the trabecular meshwork in the outflow pathway and the optic
476 nerve head have been associated with POAG[60], and have been suggested to cause impairment of

477 optic nerve axonal transport and neurotrophic supply that could influence RGC degeneration[60].
478 Regulation by the homeodomain transcription factor, VENTX, was the most significantly enriched
479 gene set for IOP genes, which has not yet been associated with glaucoma. VENTX is proposed to
480 play important roles during embryonic patterning (by homology), including in neural crest
481 development[61], as well as hematopoiesis, leukemogenesis, cellular senescence and macrophage
482 differentiation[62]. Its strongest expression in our single cell data was in lymphocytes in the anterior
483 segment, and macrophages in the optic nerve head, proposing a novel link between immune-
484 related processes and IOP levels. Reduced circulating endothelial progenitor cells has been
485 reported in POAG patients[63], which could explain impaired flow-mediated vasodilation in POAG[64].
486 Additional processes suggested to affect IOP regulation, aside from previously suggested[9] vascular
487 development, are regulation of cytoskeleton organization, and adherens junction, a cell-cell junction
488 whose cytoplasmic face is linked to the actin cytoskeleton, and that allows cells to respond to
489 biomechanical forces and structural changes in the tissue microenvironment[65]. Inhibition of
490 adherens junction regulation in trabecular meshwork has been shown to modestly influence IOP
491 levels in rabbits[66]. We also found modest enrichment of POAG genes in neuronal-related
492 processes, including genes affecting retinal morphology, sensory neuron innervation pattern, and
493 regulation of axon guidance. These genes may represent IOP-independent mechanisms, which
494 will need to be corroborated in future GWAS with larger numbers of normal tension glaucoma
495 cases.

496 In addition to prioritizing causal genes for POAG and IOP, e/sQTLs suggest the direction of
497 effect of gene expression changes or alternative splicing on disease risk that could inform drug
498 design. In this study, we provide various hypotheses of putative causal genes and regulatory
499 mechanisms that may affect POAG susceptibility in an IOP-dependent or independent manner, for
500 experimental follow up. For example, an increase in expression or alternative splicing of *TMCO1*,
501 a gene that regulates the balance of calcium ions inside the endoplasmic reticulum, or a decrease
502 in expression of *LMX1B*, LIM homeobox transcription factor 1 beta, that is essential for several
503 developmental processes including the anterior segment of the eye[67], were proposed to reduce
504 POAG risk and IOP levels. The lead IOP GWAS variant (rs116089225) in *TMCO1* that colocalized
505 with *TMCO1* e/sQTLs has been recently associated with variable number tandem repeat (VNTR)
506 length in the UK biobank study[68]. However, the VNTR did not display allelic series association with
507 *TMCO1* expression levels in GTEx[68], suggesting that the GWAS variant might be tagging more
508 than one causal mechanism. As for IOP-independent mechanisms, an sQTL acting on *CDKN2B-*
509 *AS1*, which leads to skipping of exons 2 and 3 that overlap the *CDKN2B* gene on the opposite
510 strand, is proposed as a potential mechanism of action for the protective signal found in this gene[69].

511 Skipping of these exons might render the *CDKN2B* antisense less efficient in forming a complex
512 with the *CDKN2B* RNA. Retinal Hi-C and epigenetic data further support potential roles for e/sQTL
513 effects on POAG in the retina, such as increased expression of *RERE* (arginine-glutamic acid
514 dipeptide repeats) proposed to increase POAG risk. Of note, *RERE* has also been associated with
515 VCDR[13]. Overexpression of the *RERE* protein that co-localizes with a nuclear transcription factor
516 triggers apoptosis, and its deficiency in mice causes retinal and optic nerve atrophy[70]. This study
517 also suggested a potential secondary causal gene, *PIGC* for the strongest POAG association, a
518 nonsense mutation in *MYOC*, which will need to be replicated in a larger independent POAG
519 GWAS. The *MYOC* mutation causes aggregation of misfolded myocilin proteins in the trabecular
520 meshwork, which may lead to elevated IOP levels[71]. Conversely, the enrichment of *PIGC* (that
521 encodes an endoplasmic reticulum-associated protein) expression, along with other POAG-
522 colocalizing genes, in oligodendrocytes in the optic nerve head (ONH), suggests a secondary
523 causal role for this locus in RGC support, in the posterior part of the eye.

524 There are several reasons why we may not have found colocalizing e/sQTLs for 40% of the
525 loci. First, some of the causal genes or regulatory effects may be specific to regions in the eye or
526 rare cell types for which we do not yet have representative e/sQTLs. Second, some genes may
527 affect POAG or IOP by perturbing processes only active during development or under specific
528 conditions or stimuli, not captured in adult tissues. Third, the causal variant may be another type of
529 molecular QTL not tested in this study, such as e/sQTL acting in *trans* or protein QTLs. Fourth,
530 some of the genetic associations may be tagging deleterious protein-coding variants[8]. Finally, there
531 are several limitations to Bayesian colocalization methodologies[52,53], as described in the
532 Supplementary Note.

533 By applying a novel method (ECLIPSER[38,39]) to the colocalizing e/sGenes and single
534 nucleus expression data from glaucoma-relevant eye tissues, we provided support for previously
535 implicated cell types affecting POAG development, and shed light on less well-established or novel
536 pathogenic cell types for POAG and IOP. One of the unique features of ECLIPSER, compared to
537 other single cell enrichment methods[72–76] is that it identifies cell types that are specific to a given
538 disease or trait, compared to a range of unrelated complex diseases and traits. Our results found
539 that gene expression variation in the ciliary and iris fibroblasts in the unconventional outflow
540 pathway in the anterior segment, in addition to the TM cells and Schlemm's canal cells in the
541 conventional outflow pathway, may both be key contributors to local IOP regulation and POAG risk.
542 The expression profile of the ciliary fibroblasts that was most strongly enriched for POAG genes, is
543 most similar to the 'beam cell A' defined in the single cell RNA-seq atlas of the outflow pathway in
544 van Zyl *et al*.[34] (Fig. S6B in [34]), which populates the ciliary muscle and uveal base of the TM; the

545 iris fibroblasts are most similar to 'beam cell B', and the TM fibroblasts to the JCT (juxtacanalicular
546 trabecular meshwork) cell type that resides adjacent to the Schlemm's canal. Since the role of the
547 unconventional outflow pathway in IOP homeostasis remains relatively understudied compared to
548 that of the conventional pathway[77], these findings may encourage further avenues of investigation.
549 Furthermore, the enrichment of IOP genes in pericytes, many of which are not currently associated
550 with POAG, extends our understanding of how genetic variation may be affecting IOP in the anterior
551 segment. Pericytes are mural cells that wrap around the endothelial cells that line capillary blood
552 vessels. A recent study has found reduced capillary diameter and impaired blood flow at pericyte
553 locations in mouse eyes with high IOP[78].
554 In the peripheral and macular retina, we found significant enrichment of POAG colocalizing
555 genes in astrocyte and Müller glia cells. Astrocyte and Müller glia are two types of macroglia cells
556 that interact with RGCs and blood vessels, and play an important role in retinal homeostasis,
557 including metabolic supply and structural support, maintaining the extracellular environment of the
558 neurons, and neurotransmitter transmission. Müller glia, the most common glial cell in the retina,
559 span the entire retinal layer, while astrocytes are present only in the innermost layer of the retina.
560 Several studies in animal models and patients with glaucoma[79–81] have found that astrocytes and
561 Müller glia cells become reactive at early stages of glaucomatous conditions when RGCs are intact,
562 suggesting a role for macroglia in the initiation and progression of glaucoma. POAG genes, but not
563 IOP genes, were also enriched in astrocyte types residing primarily in the ONH that contains the
564 lamina cribrosa (LC)[82], a mesh-like structure where unmyelinated RGCs pass through the sclera to
565 exit the eye, and another in the ONH and optic nerve (ON). Notably, astrocytes have been found
566 to be one of the major cell types isolated from human ONH[82] and in LC dissected from human
567 ONH[83], and make up ~20% of the cells in our ONH snRNA-seq dataset.
568 In the ONH and surrounding posterior tissues, POAG genes were most strongly enriched
569 in fibroblasts abundant in the peripapillary sclera (PPS), which surrounds the ONH. Pressure on
570 the ONH and PPS that is a continuum of the LC can cause astrocyte reactivity and compression of
571 RGC axons that can lead to RGC death[84,85] . Genes mapped to POAG, but not IOP loci were also
572 enriched in oligodendrocytes that form a myelin sheath around the axons of RGCs, and
573 oligodendrocyte precursor cells found in the ON, suggesting new IOP-independent mechanisms
574 that can affect optic nerve degeneration. The strongest enrichment for IOP was in vascular
575 endothelial (also enriched for POAG genes) and fibroblast cells primarily residing in the choroid,
576 but also in the ONH and PPS, suggesting that vascular structural abnormalities or functional
577 dysregulation of blood flow to the optic nerve and retina may be an important contributor to POAG[86].
578 It is also possible that the enrichment in the ONH vascular endothelial cells is capturing causal

579 mechanisms acting in the vascular endothelial cells in the anterior segment that were enriched for
580 most of the same IOP genes as in ONH. The IOP genes were also enriched in vascular smooth
581 muscle cells (VSMC) in the PPS and sclera. These VSMC-specific genes were enriched in lipid
582 binding and negative regulation of cell substrate adhesion processes, suggesting a role in
583 cytoskeleton-associated cell-cell adhesion and cell-extracellular matrix adhesion. These muscle
584 cells may be part of the LC, as LC cells isolated from human ONH were found to stain for alpha-
585 smooth muscle actin[82,83]. Cells in the LC produce extracellular matrix proteins to support the LC
586 structure[83], and biomechanical strain on the LC, such as from elevated IOP, is thought to be one
587 of the causes of RGC degeneration[87,88]. Further investigation will be needed to determine whether
588 the muscle cells found in the ONH single nucleus dataset[37] reside in the LC or in other structures
589 such as blood vessels.

590 Notably, we did not find significant enrichment of cell type-specific expression of POAG or
591 IOP genes in RGCs, whose cell death is the key characteristic of glaucoma, but rather in neuronal
592 support cells. This highlights the importance of targeting the support cells in new therapy design. It
593 should be noted that multiple colocalizing POAG genes are expressed in RGCs (see
594 Supplementary Fig. 20 and Monavarfeshani *et al*.[37]), however they are also expressed in other
595 retinal cell types. Hence, the potential effect of these genes on POAG via RGCs merits further
596 investigation. Furthermore, while several studies have suggested that microglia, specialized
597 macrophage-like cells, may affect RGC survival[89], we did not find support for a causal role of
598 microglia or immune cells in POAG susceptibility. A less expected result was the enrichment of
599 POAG genes in RPE cells, which was also shown in the posterior ocular cell atlas[37]. In all, our
600 findings in retina, ONH and the surrounding tissues propose cell types and biological processes
601 that may be viable targets for neuroprotective therapies.

602 A potential limitation of our GWAS-cell type enrichment method, ECLIPSER is that it only
603 considers genes that map to genome-wide significant loci and not subthreshold associations. We
604 thus provided further support for our cell type enrichment results using two additional methods,
605 stratified LD score regression and MAGMA, that analyze multiple modest associations genome-
606 wide in additional to known GWAS loci. Furthermore, ECLIPSER primarily considers genes whose
607 expression is specific to one or few cell types within a tissue, as the cell type specificity scoring
608 metric was found to be successful in identifying known pathogenic cell types for a range of complex
609 diseases and traits in a cross-tissue single nucleus expression atlas using GTEx samples[38]. We
610 note though that genes expressed at similar levels across most or all cell types may also contribute
611 to disease risk or trait variation and would be missed with this approach.

612 In conclusion, our work has generated new insights into POAG mechanisms, which could
613 inform the development of novel therapies targeting IOP reduction and neuroprotection. By
614 integrating genetic regulation and single cell expression in glaucoma-relevant ocular tissues with
615 GWAS summary statistics we have identified known and new causal genes and biological
616 processes; proposed key ocular cell types that may be pathogenic for glaucoma; and provided
617 evidence for the existence of hundreds of novel genetic associations of regulatory effects for
618 glaucoma. In the future, detection of e/sQTLs in relevant eye tissues and at the cellular level[90,91] is
619 expected to provide a more complete picture of the causal molecular and cellular mechanisms of
620 POAG risk and IOP variation.
621
622 **Methods**
623
624 **GWAS datasets.** We applied colocalization and fine-mapping analysis to 127 GWAS loci identified
625 in the cross-ancestry POAG GWAS meta-analysis of 34,179 cases and 349,321 controls from
626 European, African, and East Asian populations[8], 68 GWAS loci from the GWAS meta-analysis of
627 the European subset of 16,677 POAG cases and 199,580 controls[8], and 133 LD-independent
628 GWAS variants in 112 loci from the IOP GWAS meta-analysis of 139,555 primarily UK Biobank
629 (European) samples[9]. The GWAS meta-analysis summary statistics, which included p-value, effect
630 size and standard error, were obtained from the corresponding studies. Chromosome positions
631 were lifted over from genome build 37 (hg19) to hg38. Association results on chromosome X were
632 only available for the POAG GWAS meta-analyses (cross-ancestry and European subset).
633
634 **GTEx and EyeGEx QTL datasets.** *cis*-eQTLs and *cis*-sQTLs from 49 tissues from GTEx release
635 v8[26] and *cis*-eQTLs from peripheral retina[27] were used in this study. Summary statistics of all
636 variant-gene e/sQTL pairs tested in each of the 50 tissues, the significant e/sGenes and e/sVariants
637 at FDR<0.05, and the gene expression levels and LeafCutter[92] values are available for download
638 from the GTEx portal (URLs). The summary statistics of all variant-gene pairs tested per gene and
639 tissue was used as input to the colocalization analysis, and the LocusZoom[93] and LocusCompare
640 plots (URLs). Plots of exon and exon junction read counts were taken from the visualizations on
641 the GTEx portal (URLs). GENCODE versions 26 and 25 were used for the GTEx v8 and EyeGEx
642 studies, respectively.
643
644 **Enrichment of POAG and IOP associations among e/sQTLs using *QTLEnrich.*** To test whether
645 genome-wide significant and nominal POAG and IOP trait associations are enriched among eQTLs

646 and sQTLs, and to assess the contribution of e/sQTLs to these traits, we applied *QTLEnrich*[24,26] to
647 the POAG and IOP GWAS meta-analyses summary statistics, using eQTLs and sQTLs from the
648 49 GTEx tissues[26,27] and eQTLs from peripheral retina (EyeGEx[27]). *QTLEnrich* is a rank and
649 permutation-based method that evaluates the fold-enrichment significance of trait associations
650 among a set of e/sQTLs in a given tissue, correcting for three confounding factors: minor allele
651 frequency (MAF), distance to the target gene's transcription start site, and local LD[24] (for more
652 details see Supplementary Note). Only protein-coding and lincRNA genes were considered in this
653 analysis. Significant tissues were determined based on an Enrichment P-value that passed
654 Bonferroni correction, correcting for 50 tissues and two QTL types tested ($P<5x10^{-4}$). The adjusted
655 fold-enrichment was used to rank the significantly enriched tissues, as this statistic is not correlated
656 with tissue sample size or number of significant e/sQTLs per tissue[24], as observed with the
657 colocalization analysis (Supplementary Fig. 4). For the significant trait-tissue pairs, the fraction and
658 number of e/sVariants proposed to be associated with POAG or IOP were estimated using an
659 empirically derived, true positive rate (Adj. π_1) approach that we implemented in the latest version
660 of *QTLEnrich* (URLs), based on Storey's analytical π_1[94,95] and an empirical FDR method[94,95] (see
661 Supplementary Note).
662
663 **Colocalization analysis.** To identify a high confidence set of genes and regulatory mechanisms
664 (e/sQTLs) that may be mediating the functional mechanisms underlying known common variant
665 associations with POAG and IOP, we applied two Bayesian-based colocalization methods:
666 eCAVIAR[41] and *enloc*[42]. These methods assess the probability that co-occurring GWAS and
667 e/sQTL signals are tagging the same causal variant or haplotype, accounting for local LD and allelic
668 heterogeneity, using slightly different fine-mapping and colocalization approaches. They are
669 applied to GWAS and QTL summary-level statistics enabling the analysis of large, well-powered
670 GWAS meta-analyses, for which genotype data are not available. For the *enloc* analysis, DAP-G[42]
671 was used to perform fine-mapping of GWAS and e/sQTL loci to estimate the posterior probabilities
672 of each variant in each locus being the causal variant, while eCAVIAR has the fine-mapping feature
673 built in. We applied the two colocalization methods to 127 POAG cross-ancestry GWAS, 68 POAG
674 GWAS loci from the European subset meta-analysis, and 133 independent IOP variants (112 loci)
675 from a primarily European study (described above). Z-scores from the GWAS and GTEx e/sQTL
676 studies, computed as the effect size (beta) divided by the standard error of the effect size for each
677 variant, were used as input into eCAVIAR and DAP-G. For the retina eQTLs, we computed z-scores
678 from the variant association p-values assuming a chi-square distribution with 1 degree of freedom.

679 All GWAS loci were tested for colocalization with all eQTLs and sQTLs from 49 GTEx
680 tissues[26] and peripheral retina eQTLs[27] that had at least 5 e/sVariants (FDR<0.05) within the GWAS
681 locus LD interval. An LD window around each lead GWAS variant was defined as the chromosome
682 positions on either side containing variants within $r^2 > 0.1$, determined using 1000 Genomes Project
683 Phase 3[96] as the reference panel, and extending an additional 50kb on either side. For the IOP and
684 POAG EUR loci, LD was computed using only the European samples in 1000 Genomes Project,
685 while for the cross-ancestry POAG loci, LD was computed using the European, African, and East
686 Asian samples in 1000 Genomes. If a GWAS variant was not found in 1000 Genomes, an LD proxy
687 variant ($r^2 > 0.8$) was searched for in GTEx, and if not found, the nearest variant was used. The
688 interval boundaries and number of variants tested are reported in Supplementary Tables 7-13.
689 eCAVIAR and *enloc* analyses were applied to all common variants (MAF>1%) that fell within the
690 GWAS LD intervals and were present in both the GWAS and e/sQTL studies. The effect allele of
691 the variants in each GWAS was aligned relative to the alternative (ALT) allele that was used as the
692 effect allele in GTEx and EyeGEx. Colocalization analysis of the retina eQTLs was only performed
693 using eCAVIAR. GWAS-e/sQTL-tissue combinations with a colocalization posterior probability
694 (CLPP) above 0.01 were considered significant with eCAVIAR and/or with an RCP above 0.1 were
695 considered significant with *enloc* based on the methods' recommendations[41,42,52]. To remove
696 potential false positives, we filtered out variant, gene, tissue, trait combinations where the
697 e/sVariant with a significant colocalization result had a GWAS p-value above $1x10^{-5}$ or whose
698 e/sQTL p-values was above $1x10^{-4}$ and/or did not pass FDR<0.05 (FALSE in column
699 'Pass_QC_QTL_FDR05_P1E04_GWAS_P1E05' in Supplementary Tables 7-12). Further details
700 on the eCAVIAR and *enloc* analyses and quality control can be found in Supplementary Note.

701 **Mendelian randomization (MR).** Mendelian randomization (MR)[51] was used to provide additional
702 genetic support for a causal relationship between colocalizing e/sQTLs and POAG and/or IOP loci.
703 Significant e/sVariants were used as the instrumental variable (IV) in MR to facilitate causal
704 inference[97] (See Supplementary Note). Two sample MR was applied to the summary statistics of
705 the e/sQTLs (exposure) and POAG or IOP GWAS (outcome) for all significant colocalizing loci
706 (Supplementary Tables 7-12), using the *TwoSampleMR* and *MendelianRandomization* packages
707 in R (version 4.1.2)[98]. To avoid confounding by ancestry, MR was conducted using the European
708 ancestry subset of the POAG GWAS and the IOP GWAS, which primarily contains European
709 individuals. MR estimates were generated by calculating the Wald ratio, i.e., the variant-outcome
710 association beta divided by the variant-exposure association beta[99]. Where multiple variants
711 constituted the instrument for the candidate gene, the inverse-variance weighted (IVW) method

712 was used as the primary method for pooling variant-specific estimates[100]. Given that the IVW
713 approach assumes no horizontal pleiotropy, methods robust to violation of the exclusion-restriction
714 assumption were used as sensitivity analyses. The simple-median[101], weighted-median[101], MR-
715 Egger[102], and MR-PRESSO[103] methods were applied. Horizontal pleiotropy was tested using the
716 Egger-intercept test and the MR-PRESSO global heterogeneity test, for which $P < 0.05$ indicated
717 the presence of horizontal pleiotropy. MR associations with Benjamini-Hochberg (BH) FDR < 0.05
718 for the primary IVW/Wald ratio test were considered statistically significant. In cases where
719 horizontal pleiotropy was found based only on the MR-PRESSO global heterogeneity test, an MR
720 PRESSO outlier-corrected p-value < 0.05 was considered a significant result.

721 **Integration of retina Hi-C and epigenetic data with colocalizing POAG loci and e/sQTLs.** To
722 identify retina eQTLs or GTEx e/sQTLs that colocalized with POAG GWAS loci that may be exerting
723 their causal effect on POAG in the retina, we inspected all POAG loci in the context of chromatin
724 loops, *cis* regulatory elements (CREs) and super-enhancers (SEs) that were previously detected
725 in retina from 5 postmortem non-diseased human donor eyes[40]. The loops were calculated from
726 Hi-C (3D chromosome conformation capture) data, and the CREs and SEs from epigenetic data,
727 as described in Marchal *et al*.[40]. The lead POAG GWAS variants and their LD proxy variants
728 (r^2>0.8), the colocalizing e/sQTLs and LD proxy variants, which are also significant e/sVariants
729 (FDR<0.05), and the e/sQTL target genes were inspected for overlap or closest overlapping gene
730 with the Hi-C loops, CREs, and SEs, using the closestBed command from bedtools (v2.27.1)[104].
731 For retina eQTLs and GTEx e/sQTLs GENCODE versions 25 and 26 were used, respectively, to
732 overlap genes and TSS hg38 coordinates. Colocalizing e/sQTLs were proposed as putative causal
733 genes to POAG, if the e/sVariant overlapped one foot of the loop and the second foot overlapped
734 the gene body or TSS of the target gene. CRE and SE target genes were defined if the e/sVariant
735 and gene body or TSS of the gene overlapped the same CRE or SE. The closest target genes
736 identified using chromatin loops for the POAG cross-ancestry GWAS loci was taken from our
737 recently published Hi-C study (Supplemental Data 4 in Marchal *et al*.[40]).
738

739 **Single nucleus RNA-seq datasets and differential gene expression.** We analyzed gene
740 expression values (log(TPK+1)) from four single-nucleus (sn) RNA-seq data sets from the following
741 glaucoma-relevant regions of the eye: anterior segment[36], retina[33,36], macula[36], and optic nerve
742 head and surrounding posterior tissues[37]. All tissue samples were dissected from non-diseased
743 eye globes from post-mortem donors with no record of eye disease, and were de-identified. The
744 number of cells per cell types in each of the tissues can be found in Supplementary Table 38.

745 Differential gene expression was applied to genes expressed in at least 5% of cells in any cell type
746 cluster in each of the datasets. Here is a brief description of the four datasets:
747 **Anterior segment:** Six tissues in the anterior segment, including central cornea,
748 corneoscleral wedge (CSW), trabecular meshwork (TM), iris, ciliary body (CB) and lens, were
749 dissected from six donors within 6 hours from death, as described in[36]. To be able to compare
750 across cell types between tissues in the anterior segment, the snRNA-seq data from cornea, CSW,
751 CB, iris, and TM were pooled, downsampled to 1000 cells per type in each tissue, and reclustered
752 yielding 34 clusters[36]. Five clusters were identified for the lens. Differential gene expression
753 analysis between each cell type and all other cell types was performed using the regression model
754 in MAST[105] that corrects for the proportion of genes expressed per cell.
755 **Retina**: Retina samples from the fovea (4mm punch), macula (6 mm punch) and/or
756 periphery were collected from six donors within 6 hours from death from the Utah Lions Eye Bank,
757 flash frozen and processed as described in[33] (more details in Supplementary Note). The number
758 of cells from the three retinal regions from each donor is given in Supplementary Table 35. snRNA-
759 seq data from RGCs from a few additional donors were added to the data set, given the relevance
760 of RGCs to glaucoma, though RGCs still only comprised about 1/250 of the total data set.
761 Differential gene expression for each cell type in the ml_class level used in this study was computed
762 using the Wilcoxon rank sum test.
763 **Macula:** Macular samples were dissected with 8mm punches from five donors within 4
764 hours of death at the University of Utah (Supplementary Table 36). For three of the samples, RGCs
765 were enriched by staining the nuclei with NEUN antibody (Millipore Sigma, #FCMAB317PE)
766 followed by FACS sorting. The macular samples were processed similarly to the optic nerve head
767 samples below. Differential gene expression for each cell type compared to all other cell types was
768 computed using the MAST method[105].
769 **Optic nerve head and posterior tissues:** The optic nerve head, including peripapillary
770 tissues, was dissected with 4 mm punches from 13 donors, the optic nerve was dissected from 7
771 donors, peripapillary sclera from 4 donors, sclera from 3 donors, and choroid from 5 donors, within
772 a median of 6 hours from death at either the University of Utah or Massachusetts General Hospital
773 (Supplementary Table 37). Further description of the tissues' dissection, single-nuclei isolation, and
774 snRNA-sequencing can be found in Supplementary Note and Monavarfeshani *et al.*[37]. snRNA-seq
775 data processing and analyses were performed similarly to the pipeline used for the anterior
776 segment in van Zyl *et al.*[36]. Thirty-six cell type clusters were identified across the five tissues.
777 Differential gene expression (DGE) was computed using the MAST method[105], comparing the cells
778 from each cell type to all other cells, excluding cells from the same cell class similar to the cell type

779 of interest, aside for the given cell type (e.g., excluding all fibroblast cell types when computing
780 DGE for cell type, 5-Fibro).
781
782 **Cell type-specific enrichment of genes that map to GWAS loci for a given complex trait using**
783 **ECLIPSER.** To identify ocular cell types that are enriched for cell type-specific expression of genes
784 mapped to GWAS loci of POAG, IOP and related traits, we extended a method we recently
785 developed called ECLIPSER (Enrichment of Causal Loci and Identification of Pathogenic cells in
786 Single Cell Expression and Regulation data)[38,39], to target genes of colocalizing e/sQTLs.
787 ECLIPSER assesses whether genes mapped to a set of GWAS loci for a given complex disease
788 or trait are enriched for cell type-specific expression compared to the cell type specificity of genes
789 mapped to a background (null) set of GWAS loci associated with hundreds of unrelated traits. The
790 underlying assumption of ECLIPSER is that multiple (though not necessarily all) trait-associated
791 genes will be more highly expressed in a given pathogenic cell type compared to non-pathogenic
792 cell types in a tissue of action, more so than unrelated traits. The analysis consisted of the following
793 main steps: **(i) Mapping genes to GWAS loci.** For the POAG and IOP traits, e/sQTL colocalization
794 analysis was used to prioritize genes in GWAS loci. For the cornea-related, VCDR and negative
795 control traits, genes were mapped to GWAS loci if they were target genes of a GTEx or retina
796 e/sQTL that was in LD (r^2>0.8) with the GWAS locus (since colocalization analysis for these traits
797 was beyond the scope of this paper). The genome-wide significant variants associated with the
798 cornea traits and negative control traits were taken from Open Targets Genetics[106], and for
799 physician and machine learning-based VCDR measures from the corresponding published GWAS
800 meta-analyses[12,13]. **(ii) Null set of GWAS loci.** We compiled a null set of GWAS loci, by selecting
801 all genome-wide significant associations for a range of complex traits in Open Targets Genetics[106]
802 that were taken from the NHGRI-EBI GWAS catalog and UK Biobank GWAS studies. We excluded
803 from the null set variants associated with any ocular trait. **(iii) LD clumping of loci.** We collapsed
804 GWAS variants that were in LD with each other (r^2>0.8) or that shared a mapped gene into a single
805 locus for the set of GWAS loci for each ocular or negative control trait and for the null set,
806 separately, to avoid inflating the cell type enrichment results due to LD[39]. **(iv) Cell type specificity**
807 **locus score.** We scored each GWAS locus for the ocular traits and the null set as the fraction of
808 genes mapped to the locus, that demonstrated cell type specificity (defined here as fold-change >
809 1.3 and FDR < 0.1). Only genes expressed in at least 5% of cells in any cell type cluster were
810 included in the analysis. **(v) Assessing cell type-specificity of GWAS locus set.** We estimated
811 a cell type specificity fold-enrichment and p-value per trait (GWAS locus set), tissue and cell type
812 combination, compared to the null GWAS locus set, using a Bayesian Fisher's exact test and the

813 95th percentile of the null locus scores for the cell type specificity cutoff. The Bayesian approach
814 enables estimating 95% confidence intervals of the fold-enrichment, including for traits that have
815 few or no loci that fall above the enrichment cutoff[39]. **(vi) Cell type specific disease-contributing**
816 **genes.** Cell type-specific genes mapped to GWAS loci whose score was equal to or above the 95th
817 percentile enrichment cutoff in significantly enriched cell types ('leading edge loci') were proposed
818 to influence the given complex trait in the given cell type ('leading edge genes'), though it is possible
819 that some of these genes are affecting the given trait through other cell types. Cell types with a
820 tissue-wide Benjamini-Hochberg FDR equal to or below 0.1, correcting for the number of cell types
821 tested per tissue, were considered significantly enriched for genes associated with a given trait. To
822 test the specificity of ECLIPSER, we applied the method to eight negative control traits listed in
823 Supplementary Table 45. To assess the robustness of the cell type enrichment results with
824 ECLIPSER, we ran two additional cell type enrichment methods of GWAS data that consider
825 genome-wide genetic associations beyond genome-wide significant loci: stratified LD score
826 regression[25] and MAGMA[107] (see below).
827
828 **Cell type specific heritability enrichment of disease associations using stratified LD score**
829 **regression.** We applied stratified LD score regression (S-LDSC)[25] (v1.0.1; URLs) to the GWAS
830 summary statistics of the POAG cross-ancestry meta-analysis, POAG European subset meta-
831 analysis and IOP meta-analysis, and the four single-nucleus differential gene expression datasets
832 described above, to evaluate the contribution of genetic variation in cell type-specific genes to trait
833 heritability. Common variants (MAF>1%) within or near genes specifically expressed in the different
834 cell types (fold-change > 1.1 and FDR<0.1) in each of the four single-nucleus eye tissue datasets
835 described above, were considered in the S-LDSC analysis. A 100 kb windows on either side of
836 each gene was used. The European samples in 1000 Genomes Project Phase 3[96] were used as
837 the reference panel for computing the LD scores for all three GWAS meta-analyses. Heritability
838 enrichment per cell type was considered significant at Benjamini-Hochberg FDR below 0.1.
839
840 **MAGMA gene-association correlation with cell type gene expression.** We applied the
841 regression-based model MAGMA (v1.10)[107] to the POAG cross-ancestry, POAG European subset,
842 and IOP GWAS meta-analyses and the four single-nucleus ocular expression datasets described
843 above, which tests for association between gene association z-scores and average gene
844 expression per cell type, controlling for average gene expression across all cell types per tissue.
845 Gene-based association z-scores were computed for each GWAS based on the most significant
846 variant (SNP-wise=top) within 100kb around each gene, as described in de Leeuw *et al.*[108]. The

847 European samples in 1000 Genomes Project Phase 3[96] were used as the reference panel for the
848 POAG EUR and IOP GWAS, while all five populations (EUR, AFR, AMR, EAS, SAS) were used
849 for the POAG cross-ancestry GWAS. Significance was determined at Benjamini-Hochberg FDR
850 below 0.1. We applied conditional analysis to all pairwise combinations of nominally significant
851 (P<0.05) cell types within a given tissue, to identify cell types whose trait association signals are
852 independent of the other significant cell type[107]. A proportional significance (PS) of the conditional
853 P-value of a cell type relative to its marginal P-value was computed for each cell type in each cell
854 type pair. Two cell types in a given pair with PS≥0.8 were considered independently associated
855 cell types, and a pair of cell types with PS≥0.5 were considered partial-joint associations. In the
856 case where one cell type had PS≥0.5 and the second cell type a conditional P-value ≥0.05, the
857 first cell type was retained and the second cell type was considered completely dependent on the
858 association of the first cell type. For more details see: https://fuma.ctglab.nl/tutorial#celltype.
859
860 **Gene set enrichment analysis of POAG and IOP associated genes.** We used *GeneEnrich*[24,26]
861 to test whether genes proposed to affect POAG risk or IOP variation cluster in specific biological
862 processes or mouse phenotype ontologies. *GeneEnrich* assesses enrichment of a set of genes of
863 interest in biological pathways or other types of biologically meaningful gene sets, using a
864 hypergeometric distribution and permutation analysis. To account for biases that could arise from
865 the set of genes expressed in a given tissue, an empirical gene set enrichment P-value was
866 computed as the fraction of 1,000 to 100,000 *k* randomly sampled genes (*k* = number of significant
867 genes, e.g., colocalizing e/sGenes) from all genes expressed in the given tissue (background set)
868 that have a hypergeometric probability equal to or higher than that of the significant list of genes.
869 Given the high LD in the HLA region on chromosome 6 (chr6:28510120-33480577) we removed
870 all genes in this region from the gene set enrichment analysis, unless noted otherwise.
871 We applied *GeneEnrich* to three groups of POAG and IOP associated genes: (i) All 228,
872 118, and 279 unique target genes of eQTLs and sQTLs that colocalized with POAG cross-ancestry,
873 POAG EUR, and IOP GWAS loci, respectively. Given that the colocalizing e/sQTLs were derived
874 from the different GTEx tissues and retina, we used all genes expressed in any of the 49 GTEx
875 tissues and retina as the background set of genes, and did not correct for expression levels given
876 the differences in expression levels between the tissues. (ii) Sets of POAG and IOP colocalizing
877 genes that were enriched in specific cell types in the eye tissues based on ECLIPSER analysis
878 (tissue-wide FDR ≤ 0.1). For the background sets of genes, we chose all genes expressed in the
879 GTEx or retina tissue that was most relevant for the enriched cell type (e.g., Brain for Optic nerve
880 head; full list in Supplementary Table 39). Given that the expression levels in a tissue may not fully

881 reflect the expression levels in the particular cell type, we did not correct for expression levels in
882 the gene set enrichment analysis of the cell type-specific gene sets. (iii) Target genes of e/sQTLs
883 (FDR<0.05) with top ranked POAG or IOP GWAS P-values (P < 0.05) in tissues whose e/sQTLs
884 were enriched for trait associations based on *QTLEnrich*. Given that e/sQTLs in most tissues
885 displayed significant enrichment, a selected set of QTL/tissue-trait pairs was chosen for gene set
886 enrichment analysis based on the tissue having a top ranked adjusted fold-enrichment and
887 consisting of cell types that may be relevant to glaucoma pathophysiology, such as cells cultured
888 fibroblasts, brain, and artery (Supplementary Tables 4-5). The background sets of genes were
889 defined as all genes expressed in the given tissue excluding the target genes of e/sQTLs with
890 GWAS P<0.05. The expression levels of the randomly sampled genes from the background set in
891 the permutation analysis were matched on the expression levels of the significant set of genes.
892 We applied *GeneEnrich* to over 11,000 gene sets from four databases downloaded from
893 MSigDB (URLs): Gene Ontology (GO) with three domains: biological processes, molecular
894 function, and cellular components; Reactome; Kyoto Encyclopedia of Genes and Genomes
895 (KEGG); and mouse phenotype ontology gene sets from the Mouse Genome Informatics (MGI).
896 Only gene sets with 10 to 1000 genes were tested, and only genes that were found in the given
897 database were included in the analysis. Statistical significance was determined using a Benjamini
898 Hochberg FDR below 0.1 per database, given extensive gene set overlap between databases.
899 Gene sets with empirical gene set enrichment below 0.05 were considered nominally significant.
900
901 **Conditional analysis of *MYOC* POAG locus**. Given our finding of significant colocalization of a
902 *PIGC* sQTL with the POAG cross-ancestry association signal in the GWAS locus rs74315329,
903 whose lead variant is a nonsense mutation in the *MYOC* gene, we tested whether there was a
904 secondary independent signal in this locus that might colocalize with the *PIGC* sQTL. We
905 performed association testing on all variants on chromosome 1 conditioning on rs74315329, the
906 lead POAG GWAS variant in the locus by applying the tool COJO (URLs) to the POAG cross-
907 ancestry GWAS meta-analysis summary statistics on chromosome 1. To maintain the *MYOC* lead
908 variant in the initial association testing we filtered out variants with MAF<0.0001. The effective
909 sample size of the POAG cross-ancestry GWAS was computed based on the equation:
910 4/[(1/Ncases)+(1/Ncontrols)][109], which yielded N=124,531 for the POAG GWAS cross-ancestry
911 meta-analysis[8]. For the variant allele frequencies required as input to COJO, we used the
912 European, African and East Asian samples in 1000 Genomes Project[96], as the POAG GWAS meta-
913 analysis is comprised of these three ancestral groups. eCAVIAR and *enloc* were applied to the
914 residual statistics in the *MOYC* locus from the conditional analysis and all overlapping e/sQTLs

from the GTEx tissues and retina. To remove potential false positives, we filtered out variant, gene, tissue, trait combinations if the e/sVariant with a significant colocalization result had a GWAS p-value above $2x10^{-5}$ or an e/sQTL p-value above $1x10^{-4}$ and/or an FDR above 0.05 (FALSE in column 'Pass_QC_QTL_FDR05_P1E04_GWAS_P2E05' in Supplementary Tables 25 and 27). We used a slightly more lenient GWAS p-value cutoff for the conditional analysis ($P<2x10^{-5}$ compared to $P<1x10^{-5}$ used for the original GWAS summary statistics) given the reduced association power of conditional analysis.

Data availability

All GTEx protected data are available through the database of Genotypes and Phenotypes (dbGaP) (accession no. phs000424.v8). The GTEx eQTL and sQTL and EyeGEx retina eQTL summary statistics are available on the GTEx portal (https://gtexportal.org/home/datasets). The snRNA-seq data for the anterior segment and macula are available in Gene Expression Omnibus (GEO) accession number GSE199013, for the optic nerve head and posterior tissues in GSE236566, and for the retina in GSE226108. The processed data of the anterior and posterior segments can be visualized in the Broad Institute's Single Cell Portal at https://singlecell.broadinstitute.org/single_cell/study/SCP1841 and https://singlecell.broadinstitute.org/single_cell/study/SCP2298. The retina Hi-C data is accessible in GEO accession number GSE202471. The GWAS summary statistics for the POAG cross-ancestry GWAS meta-analysis and European subset meta-analysis are accessible in GEO under accession numbers GCST90011770 and GCST90011766, respectively, and for IOP are available from the corresponding publication (Khawaja *et al.,* Nature Genetics 2018). The GWAS loci for complex traits analyzed in this study were downloaded from Open Targets Genetics (https://genetics.opentargets.org/). The gene sets taken from MSigDB were downloaded from: http://www.gsea-msigdb.org/gsea/msigdb/collections.jsp, and the mouse phenotype ontology gene sets from the Mouse Genome Informatics (MGI) website (http://www.informatics.jax.org/).

Code Availability

The code of all tools used for analyses in this paper are publicly available and are listed in the URLs below. Custom code used to generate some of the plots are available upon request.

URLs

GTEx: https://gtexportal.org/home/datasets

EyeGEx: https://gtexportal.org/home/datasets

QTLEnrich v2: https://github.com/segrelabgenomics/QTLEnrich
GeneEnrich v2: https://github.com/segrelabgenomics/GeneEnrich
MSigDB: http://www.gsea-msigdb.org/gsea/msigdb/collections.jsp
PLINK: https://www.cog-genomics.org/plink/
eCAVIAR: https://github.com/fhormoz/caviar
fastEnloc: https://github.com/xqwen/fastenloc
DAP-G: https://github.com/xqwen/dap/tree/master/dap_src
ECLIPSER: https://github.com/segrelabgenomics/ECLIPSER
MAGMA v1.10: https://ctg.cncr.nl/software/magma, https://fuma.ctglab.nl/tutorial#celltype
S-LDSC v1.0.1: https://github.com/bulik/ldsc
genomAD: https://gnomad.broadinstitute.org/
QMplot: https://github.com/ShujiaHuang/qmplot
LocusCompare: https://github.com/boxiangliu/locuscomparer

Acknowledgements

We thank William Wen for helpful discussions on the interpretation of the colocalization results. We thank members of the Segrè lab for valuable comments and feedback. This work was funded by NIH/NEI R01 EY031424-01 (AVS, ARH, JR, PAM), NIH/NEI P30 EY014104 (JLW, AVS), NIH/NEI EY032559-01 (JLW, AVS), and the Chan Zuckerberg Initiative (CZI) Seed Network for the Human Cell Atlas awards CZF2019-002459 (JRS, AVS, WY, AM) and CZF2019-002425 (QL, RC). XJ is supported by the University of Edinburgh and University of Helsinki joint PhD studentship program in Human Genomics. VV is supported by an MRC University Unit Programme grant (MC_UU_00007/10) (QTL in Health and Disease). APK is supported by a UK Research and Innovation Future Leaders Fellowship, an Alcon Research Institute Young Investigator Award and a Lister Institute for Preventive Medicine Award. This research was supported by the NIHR Biomedical Research Centre at Moorfields Eye Hospital and the UCL Institute of Ophthalmology.

Competing interests

APK has acted as a paid consultant or lecturer to Abbvie, Aerie, Allergan, Google Health, Heidelberg Engineering, Novartis, Reichert, Santen and Thea.

Figure 1

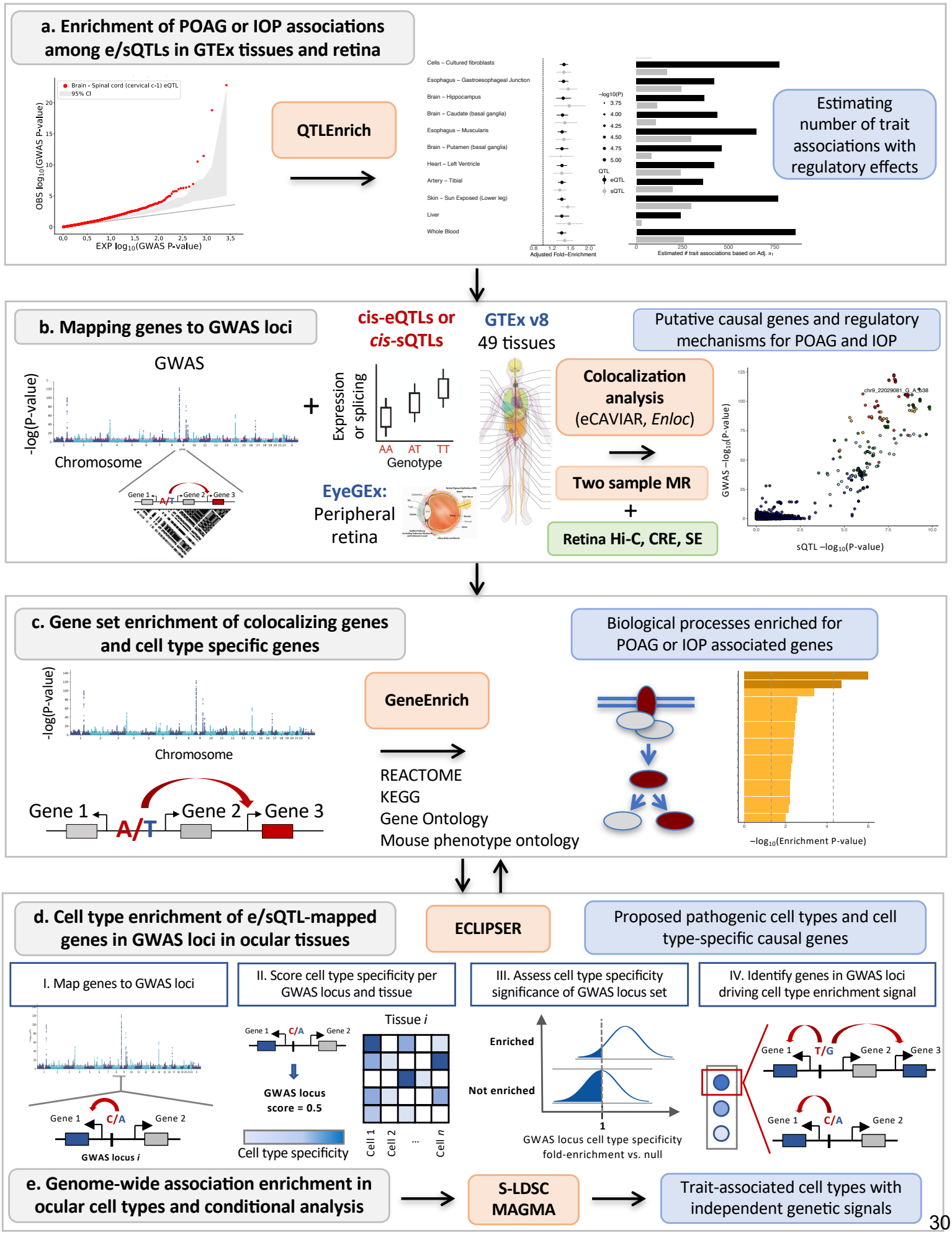
a. Enrichment of POAG or IOP associations among e/sQTLs in GTEx tissues and retina
Brain - Spinal cord (cervical c-1) eQTL
95% CI
OBS log10(GWAS P-value)
EXP log10(GWAS P-value)
QTLEnrich
Cells – Cultured fibroblasts
Esophagus – Gastroesophageal Junction
Brain – Hippocampus
Brain – Caudate (basal ganglia)
Esophagus – Muscularis
Brain – Putamen (basal ganglia)
Heart – Left Ventricle
Artery – Tibial
Skin – Sun Exposed (Lower leg)
Liver
Whole Blood
Adjusted Fold–Enrichment
–log10(P)
QTL
eQTL
sQTL
Estimated # trait associations based on Adj. P
Estimating number of trait associations with regulatory effects
b. Mapping genes to GWAS loci
GWAS
-log(P-value)
Chromosome
Gene 1
Gene 2
Gene 3
A/T
cis-eQTLs or cis-sQTLs
Expression or splicing
AA
AT
TT
Genotype
GTEx v8
49 tissues
EyeGEx:
Peripheral retina
Colocalization analysis
(eCAVIAR, Enloc)
Two sample MR
Retina Hi-C, CRE, SE
Putative causal genes and regulatory mechanisms for POAG and IOP
GWAS –log10(P-value)
sQTL –log10(P-value)
c. Gene set enrichment of colocalizing genes and cell type specific genes
-log(P-value)
Chromosome
Gene 1
Gene 2
Gene 3
A/T
GeneEnrich
REACTOME
KEGG
Gene Ontology
Mouse phenotype ontology
Biological processes enriched for POAG or IOP associated genes
–log10(Enrichment P-value)
d. Cell type enrichment of e/sQTL-mapped genes in GWAS loci in ocular tissues
ECLIPSER
Proposed pathogenic cell types and cell type-specific causal genes
I. Map genes to GWAS loci
II. Score cell type specificity per GWAS locus and tissue
III. Assess cell type specificity significance of GWAS locus set
IV. Identify genes in GWAS loci driving cell type enrichment signal
Gene 1
C/A
Gene 2
GWAS locus i
GWAS locus score = 0.5
Cell type specificity
Tissue i
Cell 1
Cell 2
...
Cell n
Enriched
Not enriched
1
GWAS locus cell type specificity fold-enrichment vs. null
T/G
e. Genome-wide association enrichment in ocular cell types and conditional analysis
S-LDSC
MAGMA
Trait-associated cell types with independent genetic signals

1016 **Figure 1. Analysis workflow from POAG and IOP GWAS to causal regulatory mechanisms,**
1017 **genes, pathways, and cell types. a,** POAG and IOP associations genome-wide (known and
1018 modest associations) were tested for enrichment among e/sQTLs in GTEx tissues and retina
1019 compared to permuted null sets of variants matched on confounding factors, using *QTLEnrich*. In
1020 cases where enrichment was found, the lower bound number of e/sQTLs in a given tissue, likely to
1021 be true trait associations was estimated using an empirically derived, true positive rate (π_1)
1022 approach. **b,** Putative causal genes were prioritized per known POAG and IOP GWAS locus by
1023 applying two colocalization methods to all e/sQTLs from 49 GTEx tissues and retina eQTLs that
1024 overlapped each locus. A Manhattan plot of the POAG cross-ancestry GWAS meta-analysis was
1025 plotted with QMplot (URLs). **c,** All target genes of significantly colocalizing e/sQTLs per trait were
1026 tested for enrichment in signaling and metabolic pathways (Reactome, KEGG), gene ontologies
1027 and mouse phenotype ontologies using *GeneEnrich*. **d,** Significantly colocalizing e/sGenes were
1028 tested for enrichment in specific cell types in single nucleus RNA-seq data of glaucoma-relevant
1029 eye tissues, using ECLIPSER. Cell type specific genes were defined with cell type fold-change
1030 >1.3 and FDR<0.1 per tissue. Cell type specificity significance per GWAS locus set for a given trait
1031 was assessed against a null distribution of GWAS loci associated with unrelated, non-ocular traits,
1032 using a Bayesian Fisher's exact test. Genes mapped to GWAS loci with a cell type specificity score
1033 above the 95th percentile of null locus scores were proposed as contributing to the trait in the
1034 enriched cell type. **e,** Cell type enrichment for the POAG and IOP GWAS was corroborated using
1035 two regression-based methods that assess cell type specificity of trait associations considering all
1036 associations genome-wide: stratified-LD score regression and MAGMA.
1037
1038
1039
1040
1041
1042
1043
1044
1045
1046
1047
1048
1049

Figure 2

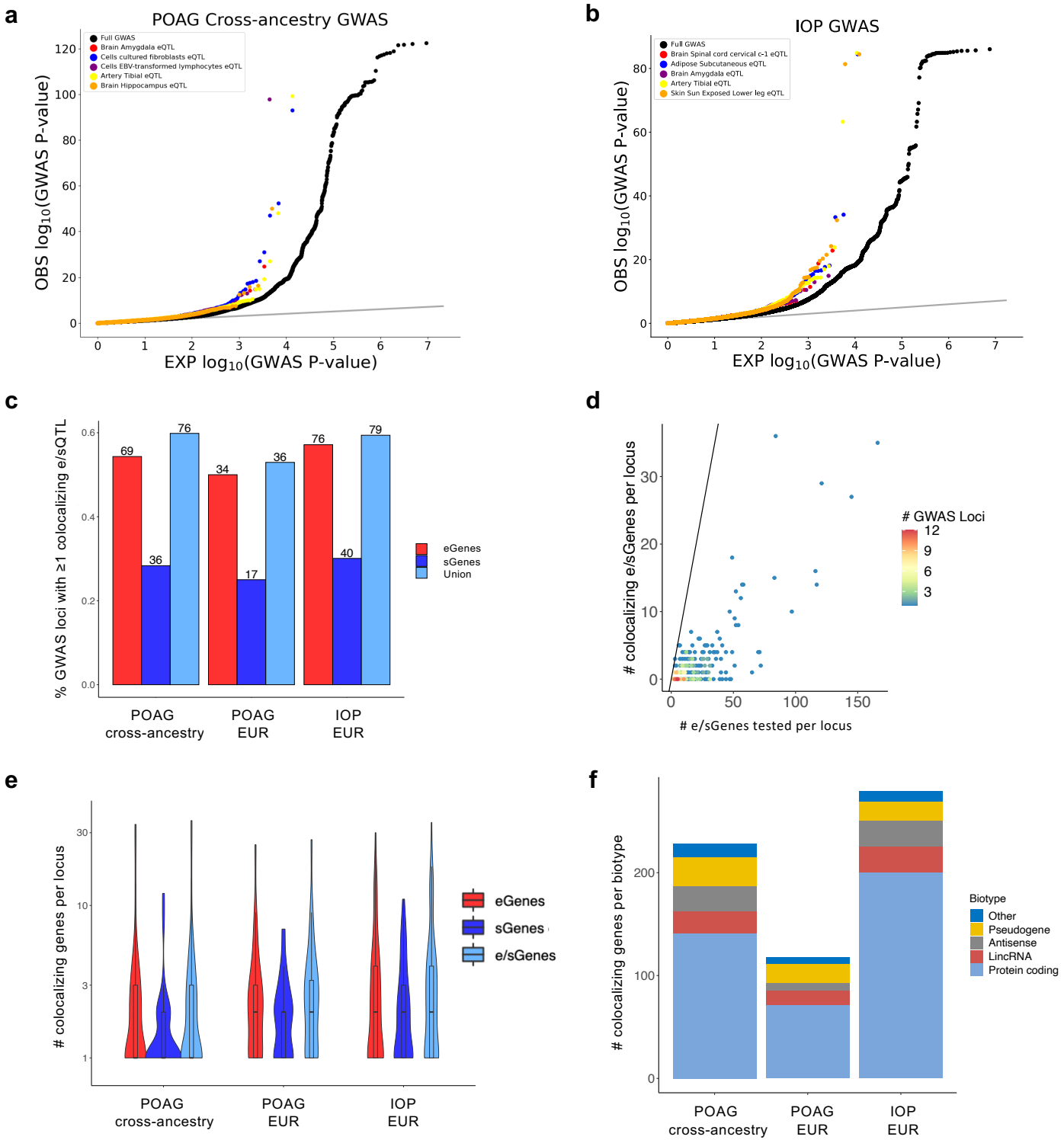
a
POAG Cross-ancestry GWAS
Full GWAS
Brain Amygdala eQTL
Cells cultured fibroblasts eQTL
Cells EBV-transformed lymphocytes eQTL
Artery Tibial eQTL
Brain Hippocampus eQTL
OBS log10(GWAS P-value)
EXP log10(GWAS P-value)
b
IOP GWAS
Full GWAS
Brain Spinal cord cervical c-1 eQTL
Adipose Subcutaneous eQTL
Brain Amygdala eQTL
Artery Tibial eQTL
Skin Sun Exposed Lower leg eQTL
OBS log10(GWAS P-value)
EXP log10(GWAS P-value)
c
% GWAS loci with ≥1 colocalizing e/sQTL
69
36
76
34
17
36
76
40
79
eGenes
sGenes
Union
POAG cross-ancestry
POAG EUR
IOP EUR
d
colocalizing e/sGenes per locus
e/sGenes tested per locus
GWAS Loci
12
9
6
3
e
colocalizing genes per locus
eGenes
sGenes
e/sGenes
POAG cross-ancestry
POAG EUR
IOP EUR
f
colocalizing genes per biotype
Biotype
Other
Pseudogene
Antisense
LincRNA
Protein coding
POAG cross-ancestry
POAG EUR
IOP EUR

Figure 2. Enrichment and colocalization analysis of eQTLs and sQTLs with POAG and IOP associations. a, b Quantile-quantile (Q-Q) plots of POAG cross-ancestry (**a**) and IOP (**b**) GWAS $-\log_{10}$ (P-value) compared to expectation for the best eQTL per eGene sets (eVariants with FDR < 0.05) of the top enriched tissues based on adjusted fold-enrichment (colored points), compared to all variants in the GWAS (black points). Grey line represents the diagonal. **c**, Histogram of percent of GWAS loci with at least one colocalizing e/sQTL (eCAVIAR CLPP > 0.01 and/or *enloc* RCP > 0.1) for the three traits (POAG cross-ancestry, POAG European (EUR) ancestry subset, and IOP European ancestry). Numbers above the bars represent the number of loci with at least one colocalizing e/sQTL. Red, dark blue, and light blue bars indicate percentage of loci with at least one colocalizing eGene, sGene, or both, respectively. **d**, Scatter plot comparing unique number of e/sGenes per locus that significantly colocalized per locus versus unique number of e/sGenes tested per locus. Points are color-coded by number of GWAS loci. The black line represents the diagonal. **e**, Violin plots showing the distribution of the unique number of colocalizing eGenes (red), sGenes (dark blue), or both (light blue) per locus for the three GWAS tested. The center line in the box plots contained within each violin plot shows the median and the box edges depict the interquartile range. **f**, Stacked histogram showing the number of colocalizing e/sGenes per gene biotype for each GWAS. Protein coding (light blue), lincRNA (brown), antisense (grey), pseudogenes (yellow), and other (dark blue).

Figure 3

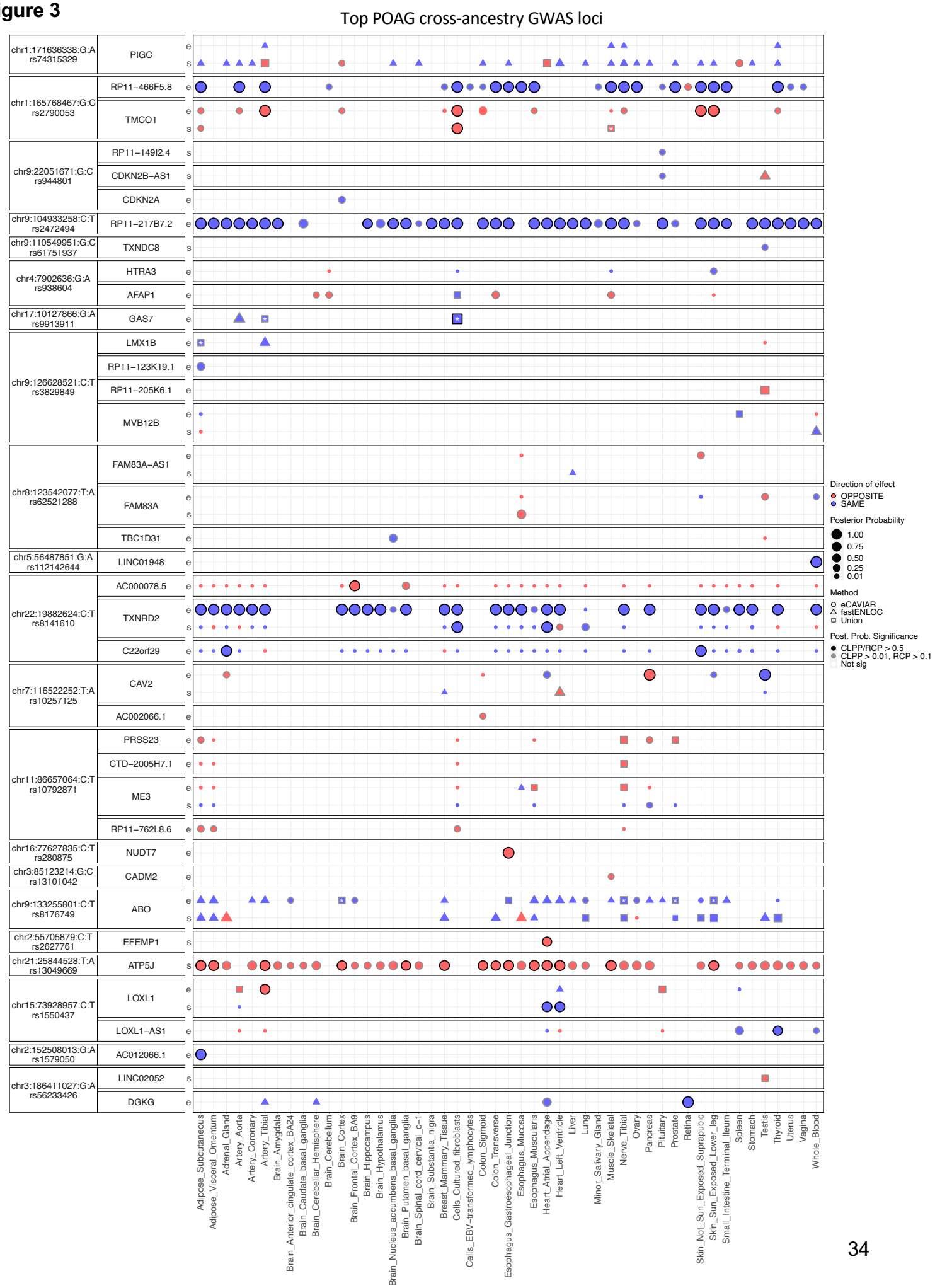
Top POAG cross-ancestry GWAS loci
chr1:171636338:G:A rs74315329
PIGC
chr1:165768467:G:C rs2790053
RP11−466F5.8
TMCO1
chr9:22051671:G:C rs944801
RP11−149I2.4
CDKN2B−AS1
CDKN2A
chr9:104933258:C:T rs2472494
RP11−217B7.2
chr9:110549951:G:C rs61751937
TXNDC8
chr4:7902636:G:A rs938604
HTRA3
AFAP1
chr17:10127866:G:A rs9913911
GAS7
chr9:126628521:C:T rs3829849
LMX1B
RP11−123K19.1
RP11−205K6.1
MVB12B
chr8:123542077:T:A rs62521288
FAM83A−AS1
FAM83A
TBC1D31
chr5:56487851:G:A rs112142644
LINC01948
chr22:19882624:C:T rs8141610
AC000078.5
TXNRD2
C22orf29
chr7:116522252:T:A rs10257125
CAV2
AC002066.1
chr11:86657064:C:T rs10792871
PRSS23
CTD−2005H7.1
ME3
RP11−762L8.6
chr16:77627835:C:T rs280875
NUDT7
chr3:85123214:G:C rs13101042
CADM2
chr9:133255801:C:T rs8176749
ABO
chr2:55705879:C:T rs2627761
EFEMP1
chr21:25844528:T:A rs13049669
ATP5J
chr15:73928957:C:T rs1550437
LOXL1
LOXL1−AS1
chr2:152508013:G:A rs1579050
AC012066.1
chr3:186411027:G:A rs56233426
LINC02052
DGKG
Adipose_Subcutaneous
Adipose_Visceral_Omentum
Adrenal_Gland
Artery_Aorta
Artery_Coronary
Artery_Tibial
Brain_Amygdala
Brain_Anterior_cingulate_cortex_BA24
Brain_Caudate_basal_ganglia
Brain_Cerebellar_Hemisphere
Brain_Cerebellum
Brain_Cortex
Brain_Frontal_Cortex_BA9
Brain_Hippocampus
Brain_Hypothalamus
Brain_Nucleus_accumbens_basal_ganglia
Brain_Putamen_basal_ganglia
Brain_Spinal_cord_cervical_c−1
Brain_Substantia_nigra
Breast_Mammary_Tissue
Cells_Cultured_fibroblasts
Cells_EBV−transformed_lymphocytes
Colon_Sigmoid
Colon_Transverse
Esophagus_Gastroesophageal_Junction
Esophagus_Mucosa
Esophagus_Muscularis
Heart_Atrial_Appendage
Heart_Left_Ventricle
Liver
Lung
Minor_Salivary_Gland
Muscle_Skeletal
Nerve_Tibial
Ovary
Pancreas
Pituitary
Prostate
Retina
Skin_Not_Sun_Exposed_Suprapubic
Skin_Sun_Exposed_Lower_leg
Small_Intestine_Terminal_Ileum
Spleen
Stomach
Testis
Thyroid
Uterus
Vagina
Whole_Blood
Direction of effect
OPPOSITE
SAME
Posterior Probability
1.00
0.75
0.50
0.25
0.01
Method
eCAVIAR
fastENLOC
Union
Post. Prob. Significance
CLPP/RCP > 0.5
CLPP > 0.01, RCP > 0.1
Not sig

1150 **Figure 3. Colocalizing e/sQTLs in GTEx tissues and retina with top POAG GWAS loci.** Genes
1151 with at least one significant colocalization result are shown for e/sQTLs tested across 49 GTEx
1152 tissues and peripheral retina for the top 21 POAG cross-ancestry GWAS loci. GWAS loci were
1153 ordered by absolute value of their effect size. Within each locus, genes were ordered based on
1154 their chromosome position. Bubble size is proportional to the maximum colocalization posterior
1155 probability of all e/sVariants tested for the given gene, QTL type and tissue combination. Points are
1156 color-coded by direction of effect (blue if increased expression or splicing increases POAG risk or
1157 vice versa; red if increased expression or splicing decreases POAG risk or vice versa). Shape of
1158 points indicates colocalization method used: circle (eCAVIAR), triangle (*enloc*), and square (tested
1159 in both methods; results shown for method with maximum posterior probability). Grey or black
1160 border denotes variant-gene-tissue-QTL combination that passed QC filtering (Methods) and a
1161 colocalization posterior probability cutoff above 0.01/0.1 (CLPP/RCP) or 0.5 (higher confidence),
1162 respectively. White or black asterisk in the square indicates whether the second method tested
1163 passed a posterior probability cutoff 0.01/0.1 (CLPP/RCP) or 0.5, respectively.
1164
1165
1166
1167
1168
1169
1170
1171
1172
1173
1174
1175
1176
1177
1178
1179
1180
1181
1182
1183

Figure 4

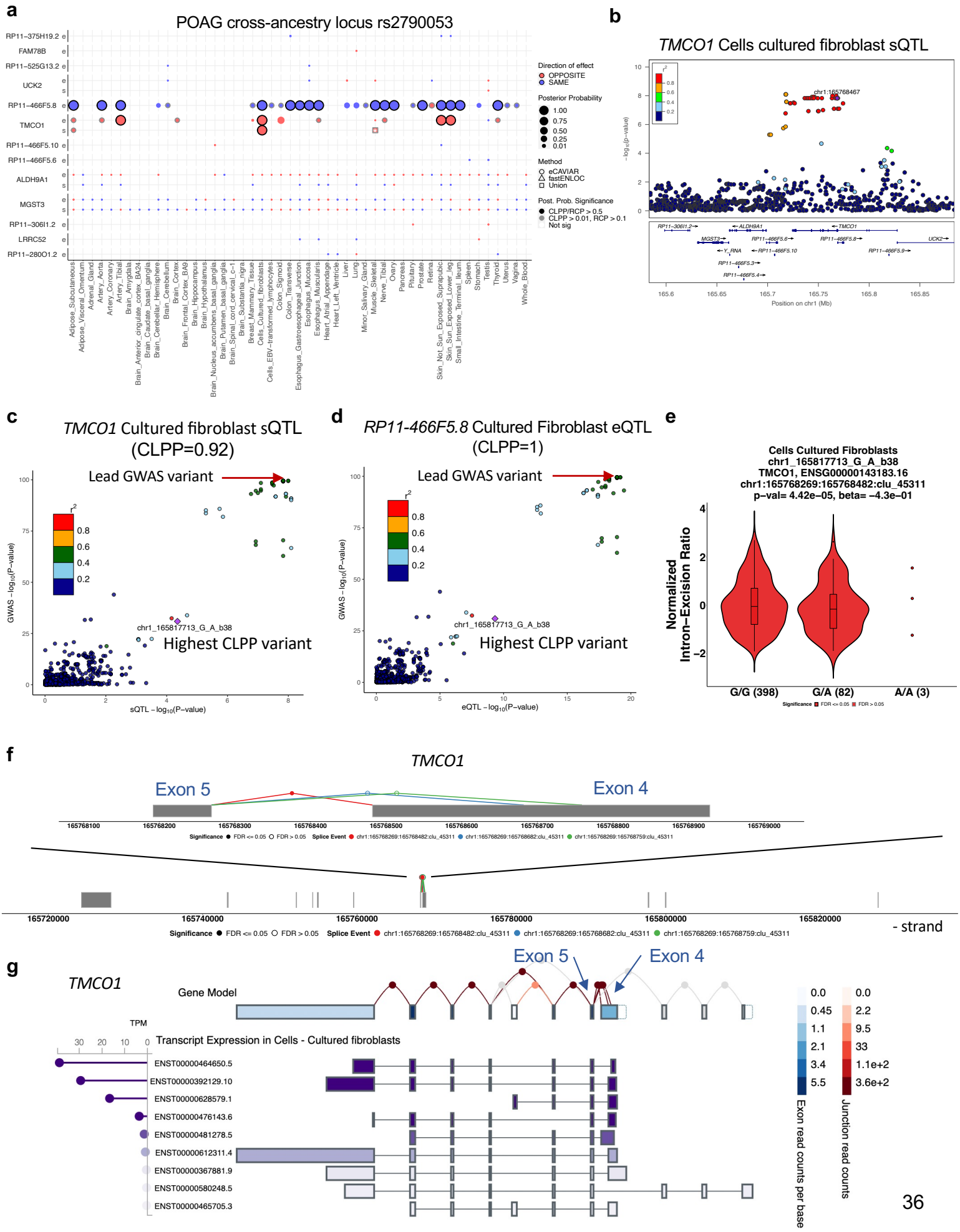
a
POAG cross-ancestry locus rs2790053
RP11−375H19.2
FAM78B
RP11−525G13.2
UCK2
RP11−466F5.8
TMCO1
RP11−466F5.10
RP11−466F5.6
ALDH9A1
MGST3
RP11−306I1.2
LRRC52
RP11−280O1.2
Direction of effect
OPPOSITE
SAME
Posterior Probability
1.00
0.75
0.50
0.25
0.01
Method
eCAVIAR
fastENLOC
Union
Post. Prob. Significance
CLPP/RCP > 0.5
CLPP > 0.01, RCP > 0.1
Not sig
b
TMCO1 Cells cultured fibroblast sQTL
chr1:165768467
Position on chr1 (Mb)
c
TMCO1 Cultured fibroblast sQTL
(CLPP=0.92)
Lead GWAS variant
chr1_165817713_G_A_b38
Highest CLPP variant
GWAS − log10(P−value)
sQTL − log10(P−value)
d
RP11-466F5.8 Cultured Fibroblast eQTL
(CLPP=1)
Lead GWAS variant
chr1_165817713_G_A_b38
Highest CLPP variant
GWAS − log10(P−value)
eQTL − log10(P−value)
e
Cells Cultured Fibroblasts
chr1_165817713_G_A_b38
TMCO1, ENSG00000143183.16
chr1:165768269:165768482:clu_45311
p−val= 4.42e−05, beta= −4.3e−01
Normalized
Intron−Excision Ratio
G/G (398)
G/A (82)
A/A (3)
f
TMCO1
Exon 5
Exon 4
- strand
g
TMCO1
Gene Model
Exon 5
Exon 4
TPM
Transcript Expression in Cells - Cultured fibroblasts
ENST00000464650.5
ENST00000392129.10
ENST00000628579.1
ENST00000476143.6
ENST00000481278.5
ENST00000612311.4
ENST00000367881.9
ENST00000580248.5
ENST00000465705.3
Exon read counts per base
Junction read counts

1217 **Figure 4. Examples of colocalizing e/sQTLs with top POAG and IOP GWAS loci. a**,
1218 Colocalization results for all e/sGenes tested in the POAG cross-ancestry rs2790053 locus LD
1219 interval with ≥1 significant eQTL or sQTL result across 49 GTEx tissues and peripheral retina based
1220 on eCAVIAR and/or *enloc*. Genes were ordered by chromosome position. Size of points is
1221 proportional to the maximum colocalization posterior probability of all e/sVariants tested for the
1222 given gene, QTL type and tissue combination. Points are color-coded by direction of effect (blue if
1223 increased expression or splicing increases POAG risk or vice versa; red if increased expression or
1224 splicing decreases POAG risk or vice versa). Shape of points indicates colocalization method: circle
1225 (eCAVIAR), triangle (*enloc*), and square (tested in both methods; results shown for method with
1226 maximum posterior probability). Grey or black border denote variant-gene-tissue-QTL combination
1227 that passed QC filtering (Methods) and a colocalization posterior probability cutoff above 0.01/0.1
1228 (CLPP/RCP) or 0.5, respectively. White or black asterisk in the square indicates whether the
1229 second method tested passed a posterior probability cutoff of 0.01/0.1 (CLPP/RCP) or 0.5,
1230 respectively. **b**, LocusZoom[96] plot for *TMCO1* sQTL -$\log_{10}$(P-value) in GTEx Cells Cultured
1231 fibroblasts in the POAG cross-ancestry GWAS variant rs2790053 (chr1_165768467_C_G_b38) LD
1232 interval. Points are color-coded by LD (r^2) relative to the lead GWAS variant. **c**,**d** LocusCompare
1233 plot of -$\log_{10}$(P-value) of the POAG cross-ancestry GWAS meta-analysis versus the -$\log_{10}$(P-value)
1234 of the Cells Cultured fibroblast sQTL or eQTL acting on *TMCO1* (**c**) or *RP11-466F5.8* (**d**),
1235 respectively. Points are color-coded based on LD (r^2) relative to the variant with the highest
1236 eCAVIAR colocalization posterior probability (CLPP). **e,** Violin plot of normalized intron-excision
1237 ratio for chr1:165768269-165768482 computed with Leafcutter[95] for *TMCO1* in Cells Cultured
1238 fibroblasts as a function of the genotype of the sVariant chr1_165817713_G_A_b38 (rs143863391)
1239 with the highest CLPP (0.92) for this sQTL and the POAG cross-ancestry GWAS locus rs2790053.
1240 The effect size of the sQTL relative to the alternative allele (*beta* = -0.43) is in opposite direction
1241 relative to the GWAS variant (*beta* = 0.25), suggesting that decreased splicing between
1242 chr1:165768269-165768482 increases POAG risk. **f,** Gene model for *TMCO1* in GTEx fibroblasts
1243 on the negative strand showing all intron excision splicing events detected with Leafcutter in
1244 *TMCO1*. A zoom in of the splicing event (chr1:165768269-165768482; red), an alternative splice
1245 donor site on exon 4 (red versus blue or green), associated with the sVariant
1246 chr1_165817713_G_A_b38 that colocalized with POAG risk is shown. A longer exon 4 in *TMCO1*
1247 is associated with decreased risk of POAG. **g,** *TMCO1* gene model and transcripts expressed in
1248 Cells Cultured fibroblasts taken from the GTEx portal (URLs). In the gene model, exon boxes are
1249 color-coded by exon read counts per base (blue) and lines connecting exons are color-coded by
1250 exon-exon junction read counts (red). All splicing events observed in the tissue are shown,

including the alternative splice event between exon 4 and exon 5 whose genetic regulation colocalized with POAG (**c**). Below the gene model, transcript expression in Cells Cultured fibroblasts in Transcripts per Million (TPM), computed with RSEM[110], is shown in descending order.

Figure 5

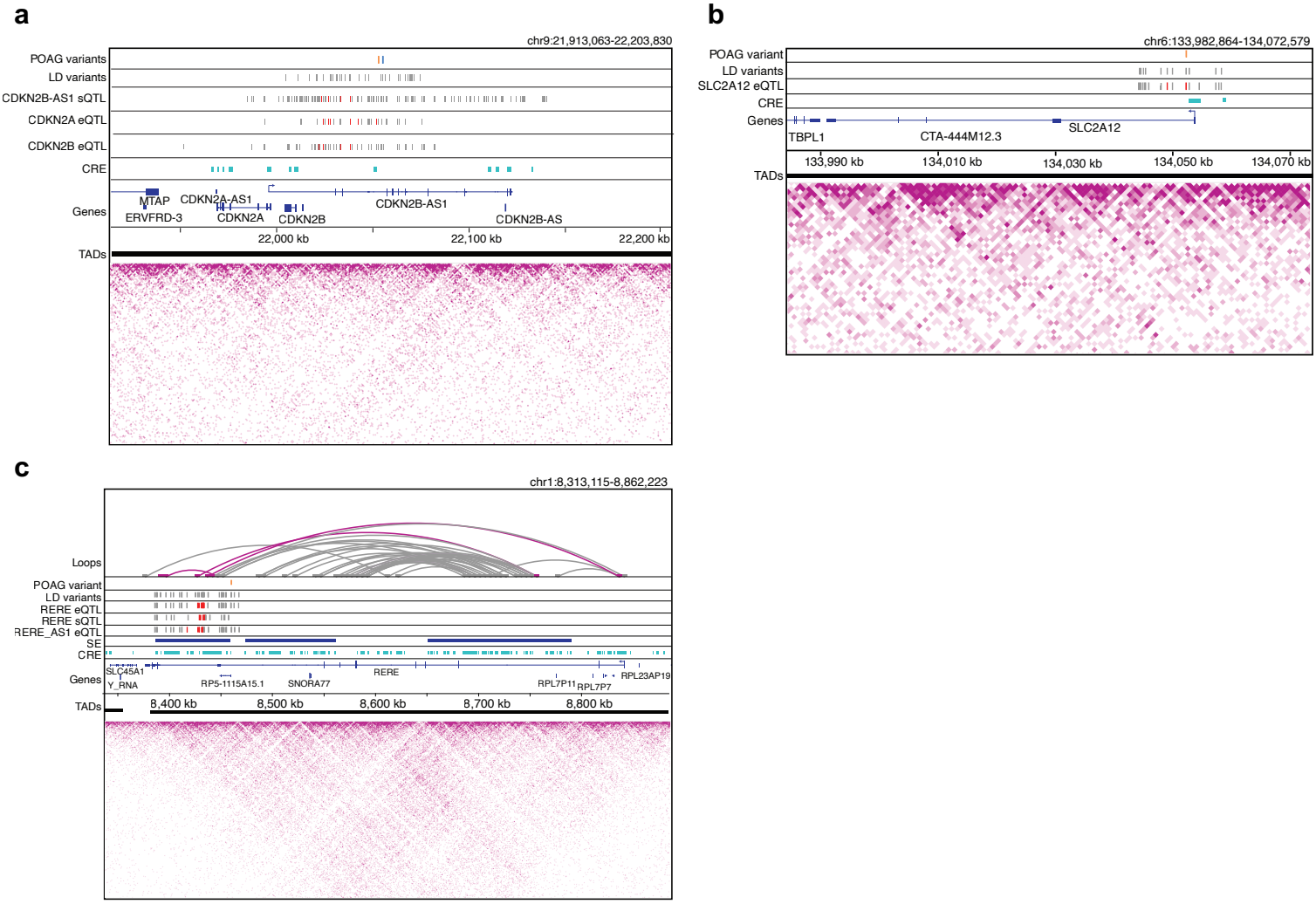
a
chr9:21,913,063-22,203,830
POAG variants
LD variants
CDKN2B-AS1 sQTL
CDKN2A eQTL
CDKN2B eQTL
CRE
Genes
MTAP
CDKN2A-AS1
CDKN2B-AS1
ERVFRD-3
CDKN2A
CDKN2B
CDKN2B-AS
22,000 kb
22,100 kb
22,200 kb
TADs
b
chr6:133,982,864-134,072,579
POAG variant
LD variants
SLC2A12 eQTL
CRE
Genes
TBPL1
CTA-444M12.3
SLC2A12
133,990 kb
134,010 kb
134,030 kb
134,050 kb
134,070 kb
TADs
c
chr1:8,313,115-8,862,223
Loops
POAG variant
LD variants
RERE eQTL
RERE sQTL
RERE_AS1 eQTL
SE
CRE
Genes
SLC45A1
Y_RNA
RP5-1115A15.1
SNORA77
RERE
RPL7P11
RPL7P7
RPL23AP19
TADs
8,400 kb
8,500 kb
8,600 kb
8,700 kb
8,800 kb

1318 **Figure 5. Chromatin loops and regulatory elements in human retina support effect of**
1319 **colocalizing e/sQTLs on POAG risk. a,** Retina CREs (cyan) derived from epigenetic data
1320 overlapping e/sVariants that colocalized with POAG associations in the *CDKN2A/B* locus. The lead
1321 POAG variants from the cross-ancestry (blue line) and European subset (orange line) GWAS are
1322 shown in the top track, followed by their linkage disequilibrium (LD) proxy variants (r^2>0.8) in the
1323 track below. The significantly colocalizing *CDKN2B-AS1* sVariants in Pituitary, *CDKN2A* eVariants
1324 in Brain Cortex, and *CDKN2B* eVariants in Skeletal Muscle are represented by red lines, and the
1325 grey lines represent LD proxy variants that are also significant e/sQTLs (FDR<0.05) for the
1326 corresponding gene and tissue. **b,** Retina CREs (cyan) overlapping retina *SLC2A12 e*Variants that
1327 colocalized with the POAG cross-ancestry association. Tracks display the lead POAG cross-
1328 ancestry GWAS variant (orange) and its LD proxy variants (grey), followed by the significantly
1329 colocalizing *SLC2A12* retina eVariants (red) with their LD proxy eVariants that are also significant
1330 eQTLs at FDR<0.05 (grey). The CRE overlaps the promoter of *SLC2A12.* **c,** Retina chromatin loops
1331 from Hi-C data, SEs (blue), and CREs (cyan) shown for the *RERE* POAG locus. Tracks display the
1332 lead POAG cross ancestry GWAS variant (orange) and its LD proxy variants (grey), followed by
1333 significantly colocalizing *RERE* eVariants in Nerve Tibial, *RERE* sVariants in fibroblast cells, and
1334 *RERE-AS1* eVariants in Adipose Subcutaneous (red), and their LD proxy variants that are also
1335 significant e/sQTLs (FDR<0.05) for the corresponding gene and tissue (grey). Magenta loops have
1336 one foot that overlaps or is in LD with the POAG variant and colocalizing e/sQTLs. In all panels,
1337 LD proxy variants were computed at r^2>0.8, TADs are represented as solid black lines, and the
1338 magenta heatmaps represent Hi-C physical contact maps. CRE, Cis-regulatory element; SE,
1339 Super-enhancer; TAD, Topologically associating domain.
1340
1341
1342
1343
1344
1345
1346
1347
1348
1349
1350
1351

Figure 6

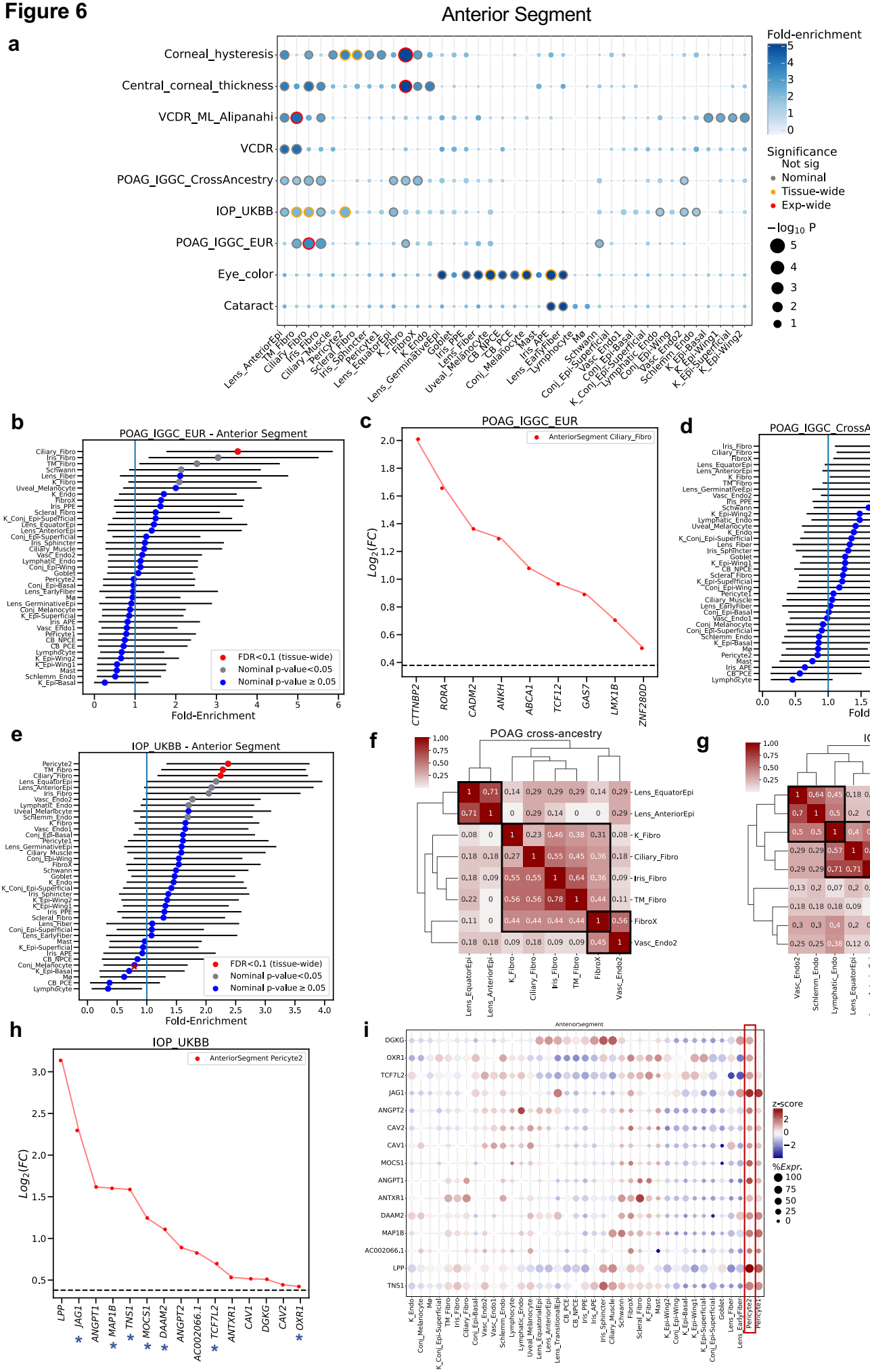
Anterior Segment
a
Corneal_hysteresis
Central_corneal_thickness
VCDR_ML_Alipanahi
VCDR
POAG_IGGC_CrossAncestry
IOP_UKBB
POAG_IGGC_EUR
Eye_color
Cataract
Fold-enrichment
Significance
Not sig
Nominal
Tissue-wide
Exp-wide
−log10 P
b
POAG_IGGC_EUR - Anterior Segment
Fold-Enrichment
FDR<0.1 (tissue-wide)
Nominal p-value<0.05
Nominal p-value ≥ 0.05
c
POAG_IGGC_EUR
AnteriorSegment Ciliary_Fibro
Log2(FC)
CTTNBP2
RORA
CADM2
ANKH
ABCA1
TCF12
GAS7
LMX1B
ZNF280D
d
POAG_IGGC_CrossAncestry - Anterior Segment
Fold-Enrichment
e
IOP_UKBB - Anterior Segment
Fold-Enrichment
f
POAG cross-ancestry
g
IOP
h
IOP_UKBB
AnteriorSegment Pericyte2
Log2(FC)
LPP
JAG1
ANGPT1
MAP1B
TNS1
MOCS1
DAAM2
ANGPT2
AC002066.1
TCF7L2
ANTXR1
CAV1
DGKG
CAV2
OXR1
i
AnteriorSegment
z-score
%Expr.

1385 **Figure 6. Cell type enrichment of e/sQTL-mapped genes for POAG, IOP and related trait loci**
1386 **in the anterior segment of the eye. a,** Significance (circle size, -log10(P-value)) and fold-
1387 enrichment (circle color) of the cell type specificity of GWAS locus sets for POAG cross-ancestry,
1388 POAR European subset, IOP, central cornea thickness, corneal hysteresis, physician-defined
1389 vertical-cup-to-disc ratio (VCDR), and machine learning (ML)-defined VCDR
1390 (VCDR_ML_Alipanahi) are shown for each of the 39 cell types found in six tissues in the anterior
1391 segment of the eye[36]. Traits (rows) and cell types (columns) were clustered based on hierarchical
1392 clustering of the euclidean distance between GWAS locus set cell type-specificity enrichment
1393 scores. Red rings: experiment-wide significant (Benjamini Hochberg (BH) FDR<0.1); Yellow rings:
1394 tissue-wide significant (BH FDR<0.1); Grey rings: nominal significant (P<0.05). **b,d,e,** Cell type
1395 specificity fold-enrichment (x-axis) in the different anterior segment cell types ranked in descending
1396 order for the POAG European subset (**b**), POAG cross-ancestry (**d**), and IOP (**e**) GWAS locus sets.
1397 Error bars: 95% confidence intervals. Red: tissue-wide significant (FDR<0.1); Grey: nominal
1398 significant (P<0.05); Blue: non-significant (P≥0.05). **c,h,** Differential gene expression (log_2(Fold-
1399 change), y axis) in the most strongly enriched cell type compared to all other cell types is shown
1400 for the set of genes (x axis) driving the enrichment signal of the POAG European GWAS loci in
1401 ciliary fibroblasts (**c**) and the IOP GWAS loci in pericytes (cluster 2) (**h**). Vertical dashed line
1402 represents log_2(Fold-change) of 0.375 (FC=1.3) and FDR<0.1 that was used as the cell type-
1403 specificity enrichment cutoff. Asterisks denote genes in IOP loci not associated with POAG risk (**h**).
1404 **f-g**, Heatmap of fraction of genes that overlap between the e/sGenes driving the enrichment signal
1405 for top ranked cell types (P<0.05) in the anterior segment for POAG cross-ancestry (**f**) and IOP (**g**)
1406 GWAS loci. Numbers refer to the fraction of e/sGenes driving the cell type enrichment on each row
1407 that overlaps with the genes driving the cell type enrichment on the corresponding column.
1408 Hierarchical clustering was performed on both rows and columns using the euclidean distance
1409 between fractions. Red asterisks: tissue-wide BH FDR<0.1. **i,** Bubble map displaying the
1410 expression of the e/sGenes driving the IOP enrichment in pericytes across all cell types in the
1411 anterior segment. The colorbar represents gene expression z-scores computed by comparing each
1412 gene's average expression in a given cell type to its per cell type average expression across all
1413 types divided by the standard deviation of all cell type expression averages. Bubble size is
1414 proportional to the percentage of cells expressing the given gene (log(TPK+1)>1). Cell type
1415 abbreviations are described in Supplementary Table 38.
1416
1417
1418

Figure 7

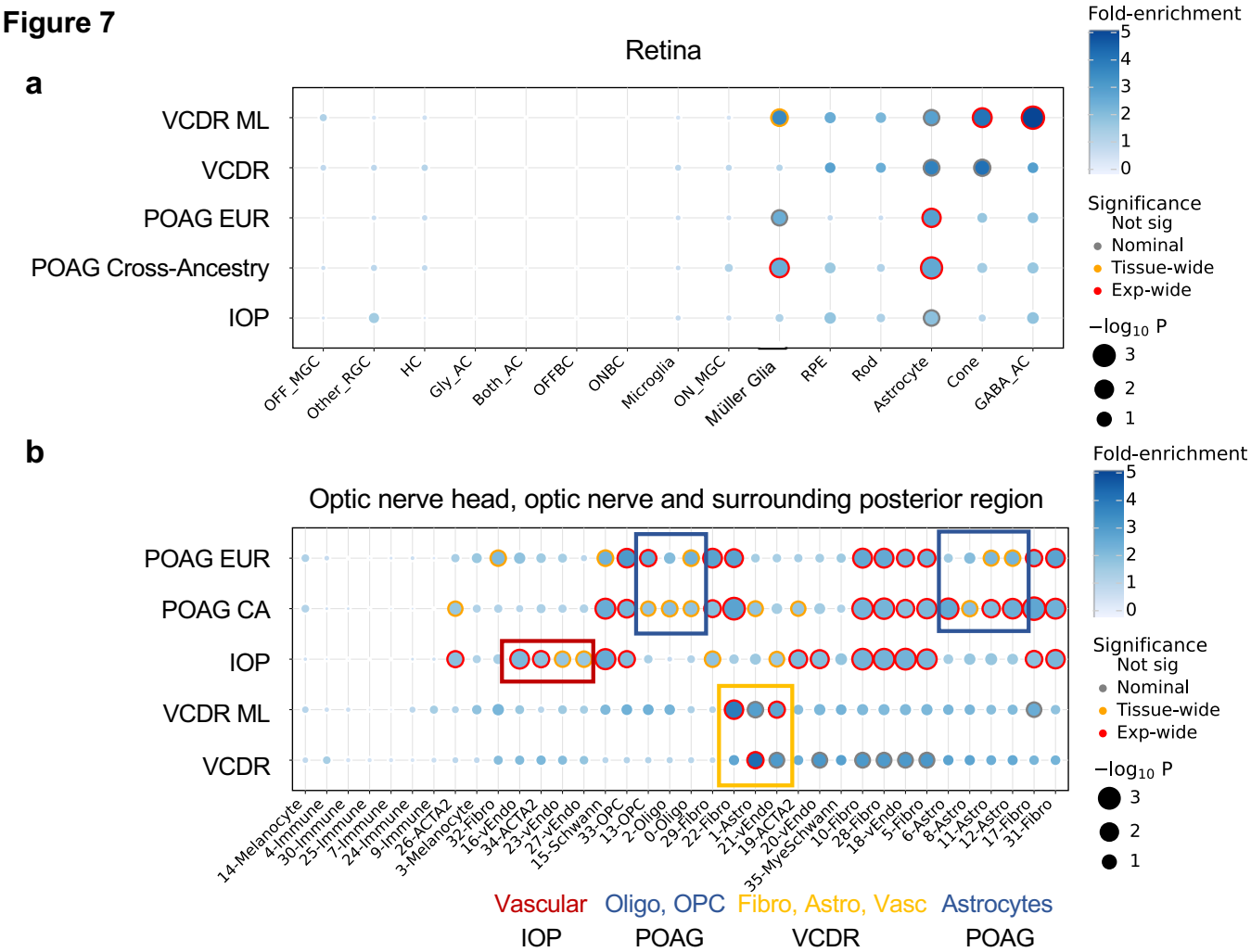
a
Retina
VCDR ML
VCDR
POAG EUR
POAG Cross-Ancestry
IOP
OFF_MGC
Other_RGC
HC
Gly_AC
Both_AC
OFFBC
ONBC
Microglia
ON_MGC
Müller Glia
RPE
Rod
Astrocyte
Cone
GABA_AC
Fold-enrichment
Significance
Not sig
Nominal
Tissue-wide
Exp-wide
−log10 P
b
Optic nerve head, optic nerve and surrounding posterior region
POAG EUR
POAG CA
IOP
VCDR ML
VCDR
Vascular
Oligo, OPC
Fibro, Astro, Vasc
Astrocytes
IOP
POAG
VCDR
POAG

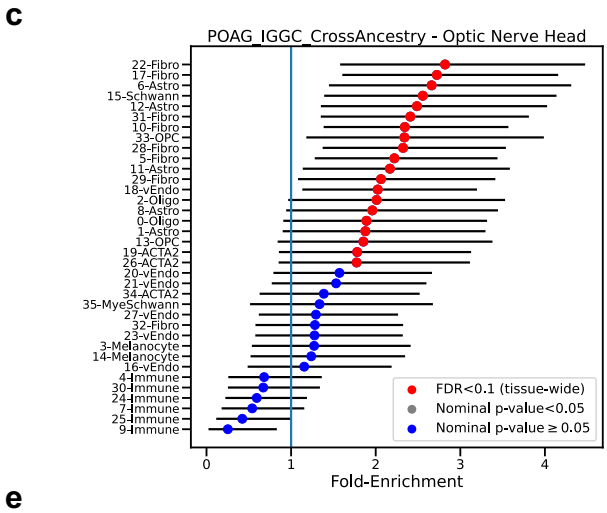
c
POAG_IGGC_CrossAncestry - Optic Nerve Head
FDR<0.1 (tissue-wide)
Nominal p-value<0.05
Nominal p-value ≥ 0.05
Fold-Enrichment

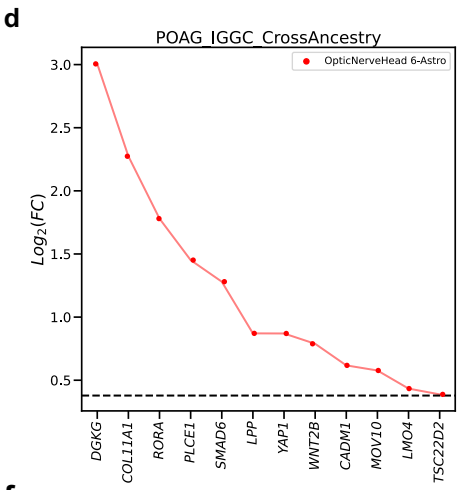
d
POAG_IGGC_CrossAncestry
OpticNerveHead 6-Astro
Log2(FC)
DGKG
COL11A1
RORA
PLCE1
SMAD6
LPP
YAP1
WNT2B
CADM1
MOV10
LMO4
TSC22D2

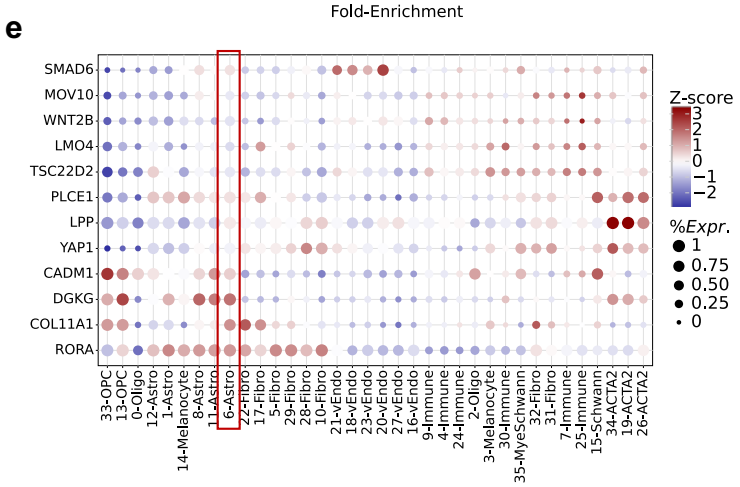
e
SMAD6
MOV10
WNT2B
LMO4
TSC22D2
PLCE1
LPP
YAP1
CADM1
DGKG
COL11A1
RORA
Z-score
%Expr.

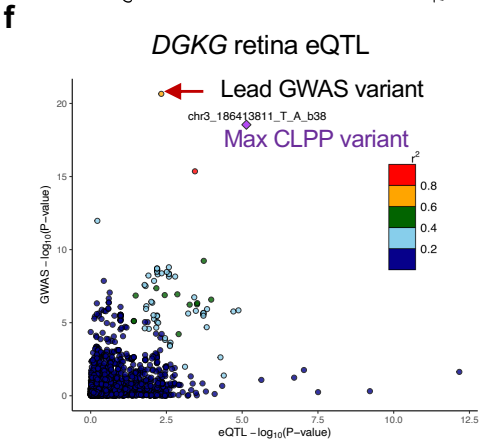
f
DGKG retina eQTL
Lead GWAS variant
chr3_186413811_T_A_b38
Max CLPP variant
GWAS −log10(P-value)
eQTL −log10(P-value)

1452 **Figure 7. Cell type enrichment of e/sQTL-mapped genes for POAG, IOP and related trait loci**
1453 **in retina, optic nerve head and surrounding tissues. a,b,** Significance (circle size, -log10(P-
1454 value)) and fold-enrichment (circle color) of the cell type specificity of GWAS locus sets for POAG
1455 cross-ancestry, POAR European subset, IOP, and physician (VCDR) and machine learning (ML)-
1456 defined VCDR (VCDR_ML_Alipanahi) are shown for each of the 15 cell types found in retina **(a)**
1457 and 36 cell types in optic nerve head (ONH), optic nerve (ON), peripapillary sclera, sclera and
1458 choroid **(b)**. Traits (rows) and cell types (columns) were clustered based on hierarchical clustering
1459 of the euclidean distance between GWAS locus set cell type-specificity enrichment scores. Red
1460 rings: experiment-wide significant (BH FDR<0.1); Yellow rings: tissue-wide significant (BH
1461 FDR<0.1); Grey rings: nominal significant (P<0.05). **c,** Cell type specificity fold-enrichment (x-axis)
1462 in the ONH and surrounding tissue cell types ranked in descending order for the POAG cross-
1463 ancestry GWAS locus set. **d,** Differential expression (log_2(Fold-change)) in astrocytes, the most
1464 strongly enriched cell type for POAG cross-ancestry GWAS loci in the ONH, compared to all other
1465 cell types in the posterior tissues is shown for the set of genes driving the POAG enrichment signal
1466 in astrocytes. Horizontal dashed line represents log_2(Fold-change) of 0.375 (FC=1.3) and FDR<0.1
1467 that was used as the cell type-specificity enrichment cutoff. **e,** The expression profile of the
1468 e/sGenes driving the POAG cross-ancestry enrichment signal in astrocytes is shown across all cell
1469 types in the ONH and surrounding tissues. Color represents z-scores computed by comparing each
1470 gene's average expression in a given cell type to the average expression across all cell types
1471 divided by its standard deviation of all cell type expression averages. Bubble size is proportional to
1472 the percentage of cells expressing the gene (log(TPK+1)>1). **f,** LocusCompare plot of -log_{10} (P-
1473 value) of the POAG cross-ancestry GWAS meta-analysis relative to -log_{10}(P-value) of a retina eQTL
1474 acting on *DGKG* that significantly colocalized with the POAG GWAS locus rs56233426
1475 (chr3_186411027_G_A). *DGKG* is the strongest astrocyte-specific gene driving the cell type
1476 enrichment signal for POAG loci. Points are color-coded based on LD (r^2) relative to the eVariant
1477 with the highest colocalization posterior probability (CLPP=0.93). The red arrow is pointing to the
1478 lead POAG GWAS variant. Cell type abbreviations are described in Supplementary Table 38.

1479 **Table 1. List of high-confidence colocalizing expression and splicing QTLs with POAG and**
1480 **IOP GWAS loci.**

GWAS locus	RS ID	GWAS effect (OR or beta)	# e/sGenes tested per locus	# significantly colocalizing e/sGenes with eCAVIAR or enloc	Colocalizing e/sGenes with eCAVIAR and *enloc* and significant with MR	Significantly colocalizing Retina eQTL	Nearest Gene	Significant in GWAS:	
POAG cross-ancestry GWAS								**IOP**	**POAG European**
chr1:171636338:G:A	rs74315329	5.46957	24	1	*PIGC (s)*	-	-	-	-
chr1:165768467:G:C	rs2790053	1.35026	13	2	*TMCO1 (e,s)*	-	+	*TMCO1*	*TMCO1*
chr9:22051671:G:C	rs944801	1.2663	26	3	*CDKN2B-AS1 (s)*	-	+	-	*CDKN2B-AS1*
chr4:7902636:G:A	rs938604	0.866407	27	2	*AFAP1 (e)*	-	+	*AFAP1*	-
chr17:10127866:G:A	rs9913911	1.14912	30	1	*GAS7 (e)*	-	+	*GAS7*	*GAS7*
chr9:126628521:C:T	rs3829849	0.87529	11	4	*LMX1B (e)*	-	+	*LMX1B*	*LMX1B*
chr7:116522252:T:A	rs10257125	0.890921	18	2	*CAV2 (e,s)*	-	-	*CAV2*	*CAV2*
chr11:86657064:C:T	rs10792871	1.12142	15	4	*PRSS23 (e), ME3 (e)*	-	+	*PRSS23, ME3*	*PRSS23, ME3*
chr9:133255801:C:T	rs8176749	1.10186	18	1	*ABO (e)*	-	+	*ABO*	-
chr15:73928957:C:T	rs1550437	0.913657	72	2	*LOXL1 (e,s)*	-	+	-	*LOXL1*
chr3:188349165:G:T	rs6787621	0.92626	7	1	*LPP (e,s)*	-	+	*LPP*	-
chr22:28712241:G:A	rs5752776	0.926631	27	5	*TTC28 (e)*	-	+	-	*TTC28*
chr2:12811195:C:T	rs12623251	0.932021	11	1	*TRIB2 (e)*	-	+	-	*TRIB2*
chr15:57261634:T:A	rs2431023	1.07026	16	2	*ZNF280D (e), TCF12 (e)*	-	+	-	*ZNF280D, TCF12*
chr11:130412183:C:T	rs2875238	0.935289	7	2	*RP11-121M22.1 (e,s), ADAMTS8 (e)*	-	+	-	-
chr7:134835770:C:A	rs10237321	0.94535	29	1	*CALD1 (e)*	-	+	-	-
chr6:134051012:G:C	rs2811688	0.946296	3	3	*SLC2A12 (e), TBPL1 (e)*	*SLC2A12*	+	-	*SLC2A12, TBPL1*
IOP GWAS								**POAG European**	**POAG cross-ancestry**
chr1:165715441:C:T	rs116089225	-0.744	29	3	*TMCO1 (e)*	-	+	*TMCO1*	*TMCO1*
chr14:74498200:C:T	rs74384554	0.417	70	4	*NPC2 (e)*	*NPC2*	-	-	*NPC2*
chr17:10127866:G:A	rs9913911	0.231	3	1	*GAS7 (e)*	-	+	*GAS7*	*GAS7*
chr7:116511284:C:T	rs10281637	-0.225	13	3	*CAV2 (e), CAV1 (e)*	-	+	*CAV2*	*CAV2*
chr11:120422429:G:A	rs11217863	-0.224	17	2	*ARHGEF12 (e,s)*	-	+	*ARHGEF12*	*ARHGEF12*
chr1:218937686:C:A	rs73103335	0.206	11	2	*LYPLAL1-AS1 (e,s)*	-	+	-	-
chr5:108710999:G:A	rs73220177	0.165	9	2	*LINC01023 (e)*	-	-	-	-
chr22:19854787:G:A	rs17534001	0.16	26	4	*TXNRD2 (e,s)*	-	+	*TXNRD2*	*TXNRD2*
chr6:170146547:G:T	rs59020521	-0.148	18	2	*RP11-302L19.3 (e)*	-	-	-	*RP11-302L19.3*
chr22:29224336:C:A	rs9608740	-0.141	40	3	*EMID1 (e,s)*	-	+	*EMID1*	-
chr2:238402728:C:T	rs57435966	0.132	25	3	*TRAF3IP1 (e)*	-	+	-	-
chr11:16989629:C:A	rs4141194	-0.131	18	5	*NCR3LG1 (e), KCNJ11 (e,s), NUCB2 (s)*	*NCR3LG1*	-	-	*NUCB2*
chr11:86699199:C:T	rs2433414	-0.128	22	6	*ME3 (e)*	-	+	*ME3*	*ME3*
chr11:47253513:G:A	rs10838681	-0.124	56	12	*PTPRJ (e)*	-	-	-	-
chr3:50162314:G:A	rs11710277	-0.12	117	14	*LSMEM2 (e)*	-	-	-	-
chr15:61659036:C:T	rs4775427	-0.111	7	5	*RP11-507B12.1 (e), RP11-507B12.2 (e), RP11-162I7.1 (e)*	-	-	*RP11-507B12.1, RP11-507B12.2, RP11-*	*RP11-507B12.1, RP11-507B12.2, RP11-*
chr14:52920118:G:C	rs8009633	0.11	12	2	*FERMT2 (e,s)*	-	+	-	-
chr2:101031432:G:A	rs55771809	0.109	17	3	*TBC1D8 (s)*	*TBC1D8*	+	-	-
chr7:116171382:C:A	rs2896175	0.108	12	4	*TES (e)*	-	-	-	-
chr16:89752083:C:T	rs3743860	0.102	57	14	*ZNF276 (e,s), SPIRE2 (e), FANCA (e,s), VPS9D1 (e)*	-	+	-	-
chr11:78374959:C:T	rs10793308	0.098	25	4	*NARS2 (e,s), USP35 (e)*	-	-	-	-
chr11:86789159:C:T	rs11606902	-0.098	12	4	*PRSS23 (e), ME3 (e)*	*PRSS23*	+	*PRSS23, ME3*	*PRSS23, ME3*
chr1:112639117:G:C	rs61818802	-0.097	14	4	*MOV10 (e), RHOC (e)*	-	-	-	*MOV10*
chr3:50143702:G:T	rs2526385	0.096	116	16	*LSMEM2 (e)*	-	-	-	-
chr22:37788844:C:T	rs6000889	0.094	47	10	*GCAT (e,s)*	-	-	-	*GCAT*
chr7:11644065:C:T	rs1635182	-0.094	4	1	*THSD7A (e)*	-	+	-	*THSD7A*
chr3:188343926:C:T	rs4132172	0.093	4	2	*LPP (e,s)*	-	+		*LPP*
chr17:46758936:C:T	rs9912530	0.091	58	14	*WNT3 (e)*	-	+	*WNT3*	-
chr1:37627051:C:T	rs4074961	-0.089	17	5	*GNL2 (e,s), MEAF6 (e), DNALI1 (s)*	*MEAF6*	-	*GNL2, MEAF6, DNALI1*	
chr10:80411803:C:T	rs6585986	-0.084	37	4	*TSPAN14 (s), ANXA11 (e)*	-	-	-	-
chr13:75683130:G:C	rs9544022	-0.081	9	2	*LMO7 (s)*	-	+	*LMO7*	-
chr2:217802649:T:A	rs3791979	-0.081	9	2	*TNS1 (e,s)*	-	+	-	-
chr11:817786:C:T	rs10902223	0.079	49	18	*PIDD1, CRACR2B, PNPLA2, CHID1*	-	-	-	-
chr10:92670768:G:A	rs9419741	-0.077	19	4	*HHEX (e)*	-	+	-	-
chr1:31726197:G:C	rs945211	-0.073	28	5	*COL16A1 (e,s)*	-	-	-	-
chr6:39895441:G:A	rs3004063	0.071	9	3	*MOCS1 (e), RP11-61I13.3 (e,s), DAAM2 (s)*	-	+	-	-
chr17:49264218:C:T	rs9899665	-0.069	31	2	*GNGT2 (e)*	-	-	-	-

1481

1482 Table lists target genes of expression and splicing QTLs (e/sGenes) that were significant based
1483 on colocalization analysis with both eCAVIAR (CLPP>0.01) and *enloc* (RCP>0.1) and Mendelian
1484 Randomization (MR) analysis (FDR<0.05) for POAG and/or IOP GWAS loci.

1485

1486 **References**

1487 1. Tham, Y.-C. *et al.* Global prevalence of glaucoma and projections of glaucoma burden
1488 through 2040: a systematic review and meta-analysis. *Ophthalmology* **121**, 2081–2090
1489 (2014).
1490 2. Weinreb, R. N. *et al.* Primary open-angle glaucoma. *Nat Rev Dis Primers* **2**, 16067 (2016).
1491 3. Leske, M. C. *et al.* Predictors of long-term progression in the early manifest glaucoma trial.
1492 *Ophthalmology* **114**, 1965–1972 (2007).
1493 4. Kwon, Y. H., Fingert, J. H., Kuehn, M. H. & Alward, W. L. M. Primary open-angle glaucoma.
1494 *N. Engl. J. Med.* **360**, 1113–1124 (2009).
1495 5. Kim, J. *et al.* Impaired angiopoietin/Tie2 signaling compromises Schlemm's canal integrity
1496 and induces glaucoma. *J. Clin. Invest.* **127**, 3877–3896 (2017).
1497 6. Costagliola, C. *et al.* How many aqueous humor outflow pathways are there? *Surv.*
1498 *Ophthalmol.* **65**, 144–170 (2020).
1499 7. Anderson, D. R., Drance, S. M., Schulzer, M. & Collaborative Normal-Tension Glaucoma
1500 Study Group. Natural history of normal-tension glaucoma. *Ophthalmology* **108**, 247–253
1501 (2001).
1502 8. Gharahkhani, P. *et al.* Genome-wide meta-analysis identifies 127 open-angle glaucoma loci
1503 with consistent effect across ancestries. *Nat. Commun.* **12**, 1258 (2021).
1504 9. Khawaja, A. P. *et al.* Genome-wide analyses identify 68 new loci associated with intraocular
1505 pressure and improve risk prediction for primary open-angle glaucoma. *Nature Genetics* vol.
1506 50 778–782 Preprint at https://doi.org/10.1038/s41588-018-0126-8 (2018).
1507 10. MacGregor, S. *et al.* Genome-wide association study of intraocular pressure uncovers new
1508 pathways to glaucoma. *Nature Genetics* vol. 50 1067–1071 Preprint at
1509 https://doi.org/10.1038/s41588-018-0176-y (2018).
1510 11. Gao, X. R. *et al.* Genome-wide association analyses identify new loci influencing intraocular
1511 pressure. *Human Molecular Genetics* vol. 27 2205–2213 Preprint at
1512 https://doi.org/10.1093/hmg/ddy111 (2018).
1513 12. Alipanahi, B. *et al.* Large-scale machine-learning-based phenotyping significantly improves
1514 genomic discovery for optic nerve head morphology. *Am. J. Hum. Genet.* **108**, 1217–1230
1515 (2021).
1516 13. Springelkamp, H. *et al.* New insights into the genetics of primary open-angle glaucoma
1517 based on meta-analyses of intraocular pressure and optic disc characteristics. *Hum. Mol.*
1518 *Genet.* **26**, 438–453 (2017).

1519 14. Lu, Y. *et al.* Common genetic variants near the Brittle Cornea Syndrome locus ZNF469
1520 influence the blinding disease risk factor central corneal thickness. *PLoS Genet.* **6**,
1521 e1000947 (2010).
1522 15. Vitart, V. *et al.* New loci associated with central cornea thickness include COL5A1, AKAP13
1523 and AVGR8. *Hum. Mol. Genet.* **19**, 4304–4311 (2010).
1524 16. Hoehn, R. *et al.* Population-based meta-analysis in Caucasians confirms association with
1525 COL5A1 and ZNF469 but not COL8A2 with central corneal thickness. *Hum. Genet.* **131**,
1526 1783–1793 (2012).
1527 17. Gao, X. *et al.* A genome-wide association study of central corneal thickness in Latinos.
1528 *Invest. Ophthalmol. Vis. Sci.* **54**, 2435–2443 (2013).
1529 18. Iglesias, A. I. *et al.* Cross-ancestry genome-wide association analysis of corneal thickness
1530 strengthens link between complex and Mendelian eye diseases. *Nat. Commun.* **9**, 1864
1531 (2018).
1532 19. Gao, X. *et al.* Genome-wide association study identifies WNT7B as a novel locus for central
1533 corneal thickness in Latinos. *Hum. Mol. Genet.* **25**, 5035–5045 (2016).
1534 20. Fan, B. J. *et al.* Family-Based Genome-Wide Association Study of South Indian Pedigrees
1535 Supports WNT7B as a Central Corneal Thickness Locus. *Invest. Ophthalmol. Vis. Sci.* **59**,
1536 2495–2502 (2018).
1537 21. Ivarsdottir, E. V. *et al.* Sequence variation at ANAPC1 accounts for 24% of the variability in
1538 corneal endothelial cell density. *Nat. Commun.* **10**, 1284 (2019).
1539 22. Simcoe, M. J., Khawaja, A. P., Hysi, P. G., Hammond, C. J. & UK Biobank Eye and Vision
1540 Consortium. Genome-wide association study of corneal biomechanical properties identifies
1541 over 200 loci providing insight into the genetic etiology of ocular diseases. *Hum. Mol. Genet.*
1542 **29**, 3154–3164 (2020).
1543 23. Han, X. *et al.* Automated AI labeling of optic nerve head enables insights into cross-ancestry
1544 glaucoma risk and genetic discovery in >280,000 images from UKB and CLSA. *Am. J. Hum.*
1545 *Genet.* **108**, 1204–1216 (2021).
1546 24. Gamazon, E. R. *et al.* Using an atlas of gene regulation across 44 human tissues to inform
1547 complex disease- and trait-associated variation. *Nat. Genet.* **50**, 956–967 (2018).
1548 25. Finucane, H. K. *et al.* Heritability enrichment of specifically expressed genes identifies
1549 disease-relevant tissues and cell types. *Nat. Genet.* **50**, 621–629 (2018).
1550 26. GTEx Consortium. The GTEx Consortium atlas of genetic regulatory effects across human
1551 tissues. *Science* **369**, 1318–1330 (2020).

1552 27. Ratnapriya, R. *et al.* Retinal transcriptome and eQTL analyses identify genes associated
1553 with age-related macular degeneration. *Nat. Genet.* **51**, 606–610 (2019).
1554 28. Strunz, T. *et al.* A mega-analysis of expression quantitative trait loci in retinal tissue. *PLoS*
1555 *Genet.* **16**, e1008934 (2020).
1556 29. Orozco, L. D. *et al.* Integration of eQTL and a single-cell atlas in the human eye identifies
1557 causal genes for age-related macular degeneration. *Cell Rep.* **30**, 1246-1259.e6 (2020).
1558 30. Liu, B. *et al.* Genetic analyses of human fetal retinal pigment epithelium gene expression
1559 suggest ocular disease mechanisms. *Commun. Biol.* **2**, 186 (2019).
1560 31. Yan, W. *et al.* Cell Atlas of The Human Fovea and Peripheral Retina. *Sci. Rep.* **10**, 9802
1561 (2020).
1562 32. Dharmat, R., Kim, S., Li, Y. & Chen, R. Single-Cell Capture, RNA-seq, and Transcriptome
1563 Analysis from the Neural Retina. *Methods Mol. Biol.* **2092**, 159–186 (2020).
1564 33. Liang, Q. *et al.* A multi-omics atlas of the human retina at single-cell resolution. *Cell Genom.*
1565 **3**, 100298 (2023).
1566 34. van Zyl, T. *et al.* Cell atlas of aqueous humor outflow pathways in eyes of humans and four
1567 model species provides insight into glaucoma pathogenesis. *Proc. Natl. Acad. Sci. U. S. A.*
1568 **117**, 10339–10349 (2020).
1569 35. Patel, G. *et al.* Molecular taxonomy of human ocular outflow tissues defined by single-cell
1570 transcriptomics. *Proc. Natl. Acad. Sci. U. S. A.* **117**, 12856–12867 (2020).
1571 36. van Zyl, T. *et al.* Cell atlas of the human ocular anterior segment: Tissue-specific and shared
1572 cell types. *Proc. Natl. Acad. Sci. U. S. A.* **119**, e2200914119 (2022).
1573 37. Monavarfeshani, A. *et al.* Transcriptomic Analysis of the Ocular Posterior Segment
1574 Completes a Cell Atlas of the Human Eye. *bioRxiv* (2023) doi:10.1101/2023.04.26.538447.
1575 38. Eraslan, G. *et al.* Single-nucleus cross-tissue molecular reference maps toward
1576 understanding disease gene function. *Science* **376**, eabl4290 (2022).
1577 39. Rouhana, J., J. Wang, G. Eraslan, S. Anand, A. Hamel, B. Cole, A. Regev, F. Aguet, K.
1578 Ardlie, and A. V. Segrè. ECLIPSER: identifying causal cell types and genes for complex
1579 traits through single cell enrichment of e/sQTL-mapped genes in GWAS loci. *BioRxiv* (2021)
1580 doi:10.1101/2021.11.24.469720.
1581 40. Marchal, C. *et al.* High-resolution genome topology of human retina uncovers super
1582 enhancer-promoter interactions at tissue-specific and multifactorial disease loci. *Nat.*
1583 *Commun.* **13**, 5827 (2022).
1584 41. Hormozdiari, F. *et al.* Colocalization of GWAS and eQTL Signals Detects Target Genes. *Am.*
1585 *J. Hum. Genet.* **99**, 1245–1260 (2016).

1586 42. Wen, X., Pique-Regi, R. & Luca, F. Integrating molecular QTL data into genome-wide
1587 genetic association analysis: Probabilistic assessment of enrichment and colocalization.
1588 *PLoS Genet.* **13**, e1006646 (2017).
1589 43. Thomson, B. R. *et al.* Angiopoietin-1 is required for Schlemm's canal development in mice
1590 and humans. *J. Clin. Invest.* **127**, 4421–4436 (2017).
1591 44. Wiggs, J. L. *et al.* Common variants at 9p21 and 8q22 are associated with increased
1592 susceptibility to optic nerve degeneration in glaucoma. *PLoS Genet.* **8**, e1002654 (2012).
1593 45. Collantes, E. R. A. *et al.* EFEMP1 rare variants cause familial juvenile-onset open-angle
1594 glaucoma. *Hum. Mutat.* **43**, 240–252 (2022).
1595 46. Wiggs, J. L. & Pasquale, L. R. Genetics of glaucoma. *Hum. Mol. Genet.* **26**, R21–R27
1596 (2017).
1597 47. Lewczuk, K., Jabłońska, J., Konopińska, J., Mariak, Z. & Rękas, M. Schlemm's canal: the
1598 outflow "vessel." *Acta Ophthalmol.* (2021) doi:10.1111/aos.15027.
1599 48. Barbeira, A. N. *et al.* Exploiting the GTEx resources to decipher the mechanisms at GWAS
1600 loci. *Genome Biol.* **22**, 49 (2021).
1601 49. Zhu, Z. *et al.* Integration of summary data from GWAS and eQTL studies predicts complex
1602 trait gene targets. *Nat. Genet.* **48**, 481–487 (2016).
1603 50. Hemani, G., Bowden, J. & Davey Smith, G. Evaluating the potential role of pleiotropy in
1604 Mendelian randomization studies. *Hum. Mol. Genet.* **27**, R195–R208 (2018).
1605 51. Zuber, V. *et al.* Combining evidence from Mendelian randomization and colocalization:
1606 Review and comparison of approaches. *Am. J. Hum. Genet.* **109**, 767–782 (2022).
1607 52. Hukku, A. *et al.* Probabilistic colocalization of genetic variants from complex and molecular
1608 traits: promise and limitations. *Am. J. Hum. Genet.* **108**, 25–35 (2021).
1609 53. Wallace, C. Eliciting priors and relaxing the single causal variant assumption in
1610 colocalisation analyses. *PLoS Genet.* **16**, e1008720 (2020).
1611 54. GTEx Consortium *et al.* Genetic effects on gene expression across human tissues. *Nature*
1612 **550**, 204–213 (2017).
1613 55. Claussnitzer, M. *et al.* FTO Obesity Variant Circuitry and Adipocyte Browning in Humans. *N.*
1614 *Engl. J. Med.* **373**, 895–907 (2015).
1615 56. Nasser, J. *et al.* Genome-wide enhancer maps link risk variants to disease genes. *Nature*
1616 **593**, 238–243 (2021).
1617 57. Cao, J. *et al.* Joint profiling of chromatin accessibility and gene expression in thousands of
1618 single cells. *Science* **361**, 1380–1385 (2018).

1619 58. Mackay, D. S., Bennett, T. M. & Shiels, A. Exome Sequencing Identifies a Missense Variant
1620 in EFEMP1 Co-Segregating in a Family with Autosomal Dominant Primary Open-Angle
1621 Glaucoma. *PLoS One* **10**, e0132529 (2015).
1622 59. Lim, S.-H. *et al.* CYP1B1, MYOC, and LTBP2 mutations in primary congenital glaucoma
1623 patients in the United States. *Am. J. Ophthalmol.* **155**, 508-517.e5 (2013).
1624 60. Fuchshofer, R. & Tamm, E. R. The role of TGF-β in the pathogenesis of primary open-angle
1625 glaucoma. *Cell Tissue Res.* **347**, 279–290 (2012).
1626 61. Scerbo, P. & Monsoro-Burq, A. H. The vertebrate-specific VENTX/NANOG gene empowers
1627 neural crest with ectomesenchyme potential. *Sci Adv* **6**, eaaz1469 (2020).
1628 62. Kumar, S., Kumar, V., Li, W. & Kim, J. Ventx Family and Its Functional Similarities with
1629 Nanog: Involvement in Embryonic Development and Cancer Progression. *Int. J. Mol. Sci.* **23**,
1630 (2022).
1631 63. Fadini, G. P. *et al.* Reduced endothelial progenitor cells and brachial artery flow-mediated
1632 dilation as evidence of endothelial dysfunction in ocular hypertension and primary open-
1633 angle glaucoma. *Acta Ophthalmol.* **88**, 135–141 (2010).
1634 64. Su, W.-W. *et al.* Glaucoma is associated with peripheral vascular endothelial dysfunction.
1635 *Ophthalmology* **115**, 1173-1178.e1 (2008).
1636 65. Green, K. J., Getsios, S., Troyanovsky, S. & Godsel, L. M. Intercellular junction assembly,
1637 dynamics, and homeostasis. *Cold Spring Harb. Perspect. Biol.* **2**, a000125 (2010).
1638 66. Pattabiraman, P. P., Epstein, D. L. & Rao, P. V. Regulation of Adherens Junctions in
1639 Trabecular Meshwork Cells by Rac GTPase and their influence on Intraocular Pressure. *J.*
1640 *Ocul. Biol. Dis. Infor.* **1**, (2013).
1641 67. Gould, D. B., Smith, R. S. & John, S. W. M. Anterior segment development relevant to
1642 glaucoma. *Int. J. Dev. Biol.* **48**, 1015–1029 (2004).
1643 68. Ronen E. Mukamel, Robert E. Handsaker, Maxwell A. Sherman, Alison R. Barton, Margaux
1644 L. A. Hujoel, Steven A. McCarroll, Po-Ru Loh. Repeat polymorphisms in non-coding DNA
1645 underlie top genetic risk loci for glaucoma and colorectal cancer. *bioRxiv* (2022)
1646 doi:10.1101/2022.10.11.22280955.
1647 69. Pasquale, L. R. *et al.* CDKN2B-AS1 genotype-glaucoma feature correlations in primary
1648 open-angle glaucoma patients from the United States. *Am. J. Ophthalmol.* **155**, 342-353.e5
1649 (2013).
1650 70. Kim, B. J. & Scott, D. A. RERE deficiency causes retinal and optic nerve atrophy through
1651 degeneration of retinal cells. *Dev. Dyn.* **250**, 1398–1409 (2021).

1652 71. Wang, H. *et al.* Physiological function of myocilin and its role in the pathogenesis of
1653 glaucoma in the trabecular meshwork (Review). *Int. J. Mol. Med.* **43**, 671–681 (2019).
1654 72. Finucane, H. K. *et al.* Partitioning heritability by functional annotation using genome-wide
1655 association summary statistics. *Nat. Genet.* **47**, 1228–1235 (2015).
1656 73. Watanabe, K., Taskesen, E., van Bochoven, A. & Posthuma, D. Functional mapping and
1657 annotation of genetic associations with FUMA. *Nat. Commun.* **8**, 1826 (2017).
1658 74. Jagadeesh, K. A. *et al.* Identifying disease-critical cell types and cellular processes across
1659 the human body by integration of single-cell profiles and human genetics. *bioRxiv*
1660 2021.03.19.436212 (2021) doi:10.1101/2021.03.19.436212.
1661 75. Slowikowski, K., Hu, X. & Raychaudhuri, S. SNPsea: an algorithm to identify cell types,
1662 tissues and pathways affected by risk loci. *Bioinformatics* **30**, 2496–2497 (2014).
1663 76. Calderon, D. *et al.* Inferring Relevant Cell Types for Complex Traits by Using Single-Cell
1664 Gene Expression. *Am. J. Hum. Genet.* **101**, 686–699 (2017).
1665 77. Stamer, W. D. & Acott, T. S. Current understanding of conventional outflow dysfunction in
1666 glaucoma. *Curr. Opin. Ophthalmol.* **23**, 135–143 (2012).
1667 78. Alarcon-Martinez, L. *et al.* Pericyte dysfunction and loss of interpericyte tunneling nanotubes
1668 promote neurovascular deficits in glaucoma. *Proc. Natl. Acad. Sci. U. S. A.* **119**, (2022).
1669 79. Wang, R., Seifert, P. & Jakobs, T. C. Astrocytes in the Optic Nerve Head of Glaucomatous
1670 Mice Display a Characteristic Reactive Phenotype. *Invest. Ophthalmol. Vis. Sci.* **58**, 924–
1671 932 (2017).
1672 80. Zhao, X., Sun, R., Luo, X., Wang, F. & Sun, X. The Interaction Between Microglia and
1673 Macroglia in Glaucoma. *Front. Neurosci.* **15**, 610788 (2021).
1674 81. Shinozaki, Y. & Koizumi, S. Potential roles of astrocytes and Müller cells in the pathogenesis
1675 of glaucoma. *J. Pharmacol. Sci.* **145**, 262–267 (2021).
1676 82. Tovar-Vidales, T., Wordinger, R. J. & Clark, A. F. Identification and localization of lamina
1677 cribrosa cells in the human optic nerve head. *Exp. Eye Res.* **147**, 94–97 (2016).
1678 83. Lopez, N. N., Clark, A. F. & Tovar-Vidales, T. Isolation and characterization of human optic
1679 nerve head astrocytes and lamina cribrosa cells. *Exp. Eye Res.* **197**, 108103 (2020).
1680 84. Strickland, R. G., Garner, M. A., Gross, A. K. & Girkin, C. A. Remodeling of the lamina
1681 cribrosa: Mechanisms and potential therapeutic approaches for glaucoma. *Int. J. Mol. Sci.*
1682 **23**, 8068 (2022).
1683 85. Calkins, D. J. Critical pathogenic events underlying progression of neurodegeneration in
1684 glaucoma. *Prog. Retin. Eye Res.* **31**, 702–719 (2012).

1685 86. Venkataraman, S. T., Flanagan, J. G. & Hudson, C. Vascular reactivity of optic nerve head
1686 and retinal blood vessels in glaucoma--a review. *Microcirculation* **17**, 568–581 (2010).
1687 87. Tamm, E. R., Ethier, C. R. & Lasker/IRRF Initiative on Astrocytes and Glaucomatous
1688 Neurodegeneration Participants. Biological aspects of axonal damage in glaucoma: A brief
1689 review. *Exp. Eye Res.* **157**, 5–12 (2017).
1690 88. Paula, J. S., O'Brien, C. & Stamer, W. D. Life under pressure: The role of ocular cribriform
1691 cells in preventing glaucoma. *Exp. Eye Res.* **151**, 150–159 (2016).
1692 89. Zeng, H.-L. & Shi, J.-M. The role of microglia in the progression of glaucomatous
1693 neurodegeneration- a review. *Int. J. Ophthalmol.* **11**, 143–149 (2018).
1694 90. Kim-Hellmuth, S., Aguet, F. & Oliva, M. Cell type–specific genetic regulation of gene
1695 expression across human tissues. (2020).
1696 91. van der Wijst, M. *et al.* The single-cell eQTLGen consortium. *Elife* **9**, (2020).
1697 92. Li, Y. I. *et al.* Annotation-free quantification of RNA splicing using LeafCutter. *Nat. Genet.* **50**,
1698 151–158 (2018).
1699 93. Pruim, R. J. *et al.* LocusZoom: regional visualization of genome-wide association scan
1700 results. *Bioinformatics* **26**, 2336–2337 (2010).
1701 94. Storey, J. D. & Tibshirani, R. Statistical significance for genomewide studies. *Proc. Natl.*
1702 *Acad. Sci. U. S. A.* **100**, 9440–9445 (2003).
1703 95. Gamazon, E. R., Huang, R. S., Dolan, M. E., Cox, N. J. & Im, H. K. Integrative genomics:
1704 quantifying significance of phenotype-genotype relationships from multiple sources of high-
1705 throughput data. *Front. Genet.* **3**, 202 (2012).
1706 96. Zheng-Bradley, X. *et al.* Alignment of 1000 Genomes Project reads to reference assembly
1707 GRCh38. *Gigascience* **6**, 1–8 (2017).
1708 97. Smith, G. D. & Ebrahim, S. "Mendelian randomization": can genetic epidemiology contribute
1709 to understanding environmental determinants of disease? *Int. J. Epidemiol.* **32**, 1–22 (2003).
1710 98. Yavorska, O. O. & Burgess, S. MendelianRandomization: an R package for performing
1711 Mendelian randomization analyses using summarized data. *Int. J. Epidemiol.* **46**, 1734–1739
1712 (2017).
1713 99. Burgess, S., Small, D. S. & Thompson, S. G. A review of instrumental variable estimators for
1714 Mendelian randomization. *Stat. Methods Med. Res.* **26**, 2333–2355 (2017).
1715 100. Burgess, S., Butterworth, A. & Thompson, S. G. Mendelian randomization analysis with
1716 multiple genetic variants using summarized data. *Genet. Epidemiol.* **37**, 658–665 (2013).

1717 101. Bowden, J., Davey Smith, G., Haycock, P. C. & Burgess, S. Consistent Estimation in
1718 Mendelian Randomization with Some Invalid Instruments Using a Weighted Median
1719 Estimator. *Genet. Epidemiol.* **40**, 304–314 (2016).
1720 102. Bowden, J., Davey Smith, G. & Burgess, S. Mendelian randomization with invalid
1721 instruments: effect estimation and bias detection through Egger regression. *Int. J. Epidemiol.*
1722 **44**, 512–525 (2015).
1723 103. Verbanck, M., Chen, C.-Y., Neale, B. & Do, R. Detection of widespread horizontal pleiotropy
1724 in causal relationships inferred from Mendelian randomization between complex traits and
1725 diseases. *Nat. Genet.* **50**, 693–698 (2018).
1726 104. Quinlan, A. R. BEDTools: The Swiss-army tool for genome feature analysis. *Curr. Protoc.*
1727 *Bioinformatics* **47**, 11.12.1-34 (2014).
1728 105. Finak, G. *et al.* MAST: a flexible statistical framework for assessing transcriptional changes
1729 and characterizing heterogeneity in single-cell RNA sequencing data. *Genome Biol.* **16**, 278
1730 (2015).
1731 106. Ghoussaini, M. *et al.* Open Targets Genetics: systematic identification of trait-associated
1732 genes using large-scale genetics and functional genomics. *Nucleic Acids Res.* **49**, D1311–
1733 D1320 (2021).
1734 107. Watanabe, K., Umićević Mirkov, M., de Leeuw, C. A., van den Heuvel, M. P. & Posthuma, D.
1735 Genetic mapping of cell type specificity for complex traits. *Nat. Commun.* **10**, 3222 (2019).
1736 108. de Leeuw, C. A., Mooij, J. M., Heskes, T. & Posthuma, D. MAGMA: generalized gene-set
1737 analysis of GWAS data. *PLoS Comput. Biol.* **11**, e1004219 (2015).
1738 109. Pollack, S. *et al.* Multiethnic Genome-Wide Association Study of Diabetic Retinopathy Using
1739 Liability Threshold Modeling of Duration of Diabetes and Glycemic Control. *Diabetes* **68**,
1740 441–456 (2019).
1741 110. Li, B. & Dewey, C. N. RSEM: accurate transcript quantification from RNA-Seq data with or
1742 without a reference genome. *BMC Bioinformatics* **12**, 323 (2011).